Assessment of Operational Non-Time Critical Sentinel-6A Michael Freilich Radio Occultation Data: Insights into Tropospheric GNSS Signal Cutoff Strategies and Processor Improvements

Saverio Paolella[1], Axel Von Engeln[1], Sebastiano Padovan[1], Riccardo Notarpietro[1], Christian Marquardt[1], Francisco Sancho[1], Veronica Rivas Boscan[1], Nicolas Morew[1], and Francisco Martin Alemany[1]

[1]EUMETSAT, Darmstadt, Germany

Correspondence: Saverio Paolella (Saverio.Paolella@external.eumetsat.int)

Abstract.

This study presents an exhaustive assessment of the Sentinel-6A Michael Freilich Radio Occultation (RO) data, focusing on the evaluation of bending angle products derived from the EUMETSAT-provided RO Non-Time Critical (RO-NTC) data collected between September and December 2021. The RO instrument has been performing very well since its launch in 2020, consistently surpassing its mission target of providing 770 quality-checked bending angle profiles per day. With a remarkable availability rate of 99.9% during full operational periods, the mission demonstrates robust performance and reliability. A detailed examination of the Signal-To-Noise Ratio (SNR) and phase noise indicates the high-quality nature of the data. The study also analyses the benefits of employing SNR-based signal cutoff strategies and L2 signal extrapolation in the troposphere, where it is more susceptible to SNR reductions. Furthermore, the paper details some processor enhancements, which led to improved bending angle statistics, particularly below 22 km altitude. Additionally, the analysis revealed terrestrial interference signals on the L2 frequency, confirming that they do not significantly compromise the Sentinel-6A RO data quality.

The validation of the EUMETSAT processed Sentinel-6A RO-NTC data against the European Centre for Medium-Range Weather Forecasts (ECMWF) short-range forecasts and comparisons with Metop-B/C and EUMETSAT-processed SPIRE occultations, highlights the reduction in random error and modifications in the tropospheric bias structure, a result of the enhancements in data processing techniques. This comprehensive analysis confirms the high quality of the EUMETSAT Sentinel-6A bending angle products and underlines the satellite's contribution to the EUMETSAT legacy of precise and reliable radio occultation data for weather forecasting and climate research.

1 Introduction

The Sentinel-6A satellite, also known as Sentinel-6 Michael Freilich, represents a significant milestone in the ongoing effort to monitor the level of Earth's oceans with altimeters. Launched on November 21st, 2020, from Vandenberg Air Force Base in California, it marks the continuation of a three-decade legacy of sea-surface height measurement that began with the TOPEX/-Poseidon mission and was carried forward by the Jason series of satellites Jason 1, 2, and 3 (Donlon et al., 2021b; Jiang et al.,

2023). Notably, Sentinel-6A is part of the Jason-CS (Continuity of Service) program, aimed at ensuring the uninterrupted collection of critical oceanographic data.

Scheduled to be joined by its sibling, Sentinel-6B, in 2025, Sentinel-6A mission is not limited to altimetry. It also includes a GNSS RO instrument called TriG (Ho et al., 2020), developed in collaboration between the National Aeronautics and Space Administration (NASA) and Jet Propulsion Laboratory (JPL). The RO technique (Melbourne et al., 1994; Kursinski et al., 1997, 2001; Hajj et al., 2002; Jakowski et al., 2009) is a powerful method used to measure the Earth's atmospheric properties, including temperature, pressure, and humidity profiles, as well as ionospheric electron density. This technique involves the transmission of radio waves from a Global Navigation Satellite System (GNSS) satellite, which are then received by a low Earth orbiting (LEO) satellite, such as Sentinel-6A. As these radio waves pass through the Earth's atmosphere, they are refracted due to the varying density and ionization levels of the atmospheric layers. The amount of this refraction provides valuable information about the atmospheric conditions along the signal's path. By precisely measuring the changes in the phase and amplitude of the received signals, one can infer the bending angle profile of the radio waves as they traverse the Earth's atmosphere. This bending angle, which is the main output of the EUMETSAT RO processors, is an important parameter that, when processed through the Abel transform (Fjeldbo et al., 1971), yields profiles of atmospheric refraction index, which in turns depends on temperature, pressure, and humidity (Smith and Weintraub, 1953) at different altitudes, as well as electron density in the ionosphere.

The RO technique offers several advantages over traditional atmospheric sounding methods. It provides global coverage, particularly when the instrument flies on polar orbits, including remote oceans and polar regions where in-situ measurements are poor or unavailable. RO measurements are not significantly affected by cloud cover or precipitation, allowing for consistent and reliable atmospheric profiling under various weather conditions. A distinct feature of the RO technique is its measurement of time, which inherently requires no calibration, thus making it a stable reference or anchor for other measurement techniques. This attribute enhances the reliability and consistency of the data obtained. The Sentinel-6A satellite, equipped with a state-of-the-art RO instrument, represents a continuation and enhancement of this observational capability, ensuring the availability of high-quality atmospheric data for weather forecasting, climate monitoring, and scientific research (Anthes, 2011; Steiner et al., 2001; Yen et al., 2010).

The Sentinel-6 RO receiver collects GNSS signals through two occultation antennas positioned in both the velocity and anti-velocity directions, for tracking rising and setting occultations respectively. The receiver is equipped also with a zenith-looking antenna dedicated to track signals for the precise orbit determination (POD) of the satellite. The occultation antennas have the capability to track both GPS L1CA/L2C/L2P and GLONASS L1/L2 signals, providing a comprehensive set of data for atmospheric profiling, while the POD antenna is exclusively focused on tracking GPS satellites. The versatility of the Sentinel-6A satellite is further highlighted by its software-configurable receiver, which allows NASA/JPL for adjustments in tracking behavior to optimize data collection based on mission needs.

This paper offers a comprehensive evaluation of the EUMETSAT processed Sentinel-6A bending angle products using the Non-Time Critical Radio Occultation (RO-NTC) data from September 1st to December 31st, 2021. NASA/JPL also provides bending angle profiles in Near-Real-Time (NRT) for which some discussions can be found in von Engeln (2024). During this

period the Sentinel-6A RO-NTC processor processed over 112,000 quality checked bending angle profiles. Approximately 62% of these occultations were from GPS signals, with the remaining being from GLONASS satellites. This distribution primarily reflects the varying sizes of the two satellite constellations, GPS with up to 32 satellites and GLONASS with nominally 24 satellites. However, several GLONASS satellites are not providing a second frequency and are thus unusable for RO (currently, affecting 3 satellites). Additionally, there is a slight imbalance between the number of setting and rising occultations, with setting occultations constituting about 53% of the total. This discrepancy can be attributed to two main reasons. The first reason is the different hardware configurations of the rising and setting occultation antennas, as detailed in Section 2. The second reason is related to the reboots of the RO instrument (some of them are reported in Section 2.1.1) which can affect the data collection and lead to variations in the number of occultations captured during different periods. Specifically, after an instrument reboot, GPS ephemeris data require more time to be downloaded by the zenith antenna, whereas GLONASS information is stored on-board. This long download time can affect the schedule of upcoming rising occultations.

The analyzed period includes the commissioning data up to November 29th 2021 and subsequent early operational data, being this date the transition day from commissioning to full operational status. As reported throughout this paper, several instrument activities and adjustments were carried out during both the commissioning and early operational phases. These efforts led to the successful achievement of the mission's target, currently providing 770 quality-checked bending angle profiles per day with a 99.9% availability rate. This milestone highlights the satellite's high operational reliability and its robust ability to deliver consistent, comprehensive data coverage.

The analysis presented in this paper extends also to the Signal-To-Noise Ratio (SNR), where findings reveal exceedingly high SNRs coupled with remarkably low phase noise. This combination is crucial for generating bending angle products of high quality.

The EUMETSAT Sentinel-6 RO processor uses the Canonical Transform 2 (CT2) algorithm, as described by (Gorbunov and Lauritsen, 2004), to retrieve bending angles from the complex field measurements along the trajectory of the LEO satellite. CT2 is part of the radio-holographic inversion methods designed to handle multipath propagation problems of RO signals in the moist lower troposphere. As (Sokolovskiy et al., 2010) reported, inversion errors are influenced by the length of recorded RO signals and their noise levels. Implementing an effective L1/L2 signals cutoff strategy, based on the SNR, is crucial in the lower troposphere to enhance the reliability of the retrieved bending angle profiles.

Furthermore, the quality of bending angles is also affected by the cutoff and extrapolation of the L2 frequency, which is more susceptible to SNR reduction in the lower troposphere. The EUMETSAT Sentinel-6 RO processor follows to the ionospheric correction procedure described in (Culverwell and Healy, 2015), which includes an improved version of the L2 cutoff strategy. The various approaches for the L2 cutoff strategy implemented by the EUMETSAT Sentinel-6 RO processor are detailed in Section 2.1.4. The effectiveness of these strategies, including the robustly fitted ionospheric model used as a reference for determining the L2 signal cutoff point, is confirmed by comparing operational data with a reprocessed version.

Enhancements applied to the Sentinel-6A RO processor for effectively removing navigation bits from the received L1/L2 GNSS signals are discussed. This will be shown to have contributed to an overall improvement of bending angles data quality when data are compared against ECMWF short-range forecasts. In addition, interference signals on the I and Q components

of the L2 frequency, not related to GNSS navigation bits, will be discussed trying to give a possible geographic localization of the interference sources.

The text is organized as follows: section 2 describes the satellite, with a focus on the RO experiment; section 2.1 provides a detailed description of the data used in this work, namely the EUMETSAT RO bending angle profiles stored in the Level 1B products, and the reference data used for their validation; section 2.1.1 is dedicated to the assessment of the daily occultation numbers and the impact of each GNSS satellite on the entire data set; section 2.1.2 focuses on the analysis on the SNRs recorded by the RO receiver for each constellation, transmitter satellite and tracked signal; section 2.1.4 reports about L2 signal cut-off strategy and extrapolation in troposphere; section 2.1.3 describes the biasing effect in troposphere related to the L1/L2 signal cut-off based on SNR; section 2.1.5 shows the impact of some improvements applied to the signal navigation bits removal algorithm on the bending angle statistics; section 2.1.6 talks about some some findings related to the presence of interference signals on the L2 frequency; section 3 presents an exhaustive validation of the bending angle profiles; section 4 provides the conclusions and a final outlook.

2 Satellite and instrument

The Sentinel-6A satellite flies in the so-called altimetry reference orbit, which was initially chosen for the TOPEX/Poseidon mission to have a good coverage of the oceans while at the same time avoiding aliasing effects among the tidal frequencies (Fu et al., 1994). It is a $66°$-inclined non-Sun-Synchronous orbit with an altitude between 1336 and 1356 km, which corresponds to a repeat cycle (i.e., the time it takes for the spacecraft to fly over the same patch of the surface) of 9.9 days (Donlon et al., 2021b, a). For the RO instrument, this translates to a local solar time coverage that does not present the clear pattern typical of sun-synchronous orbits. Figure 1 illustrates this point by combining RO events distributions for the Sentinel-6A and the EUMETSAT Polar System (EPS) Meteorological Operational (Metop) satellites, these latter flying on a $98.7°$-inclined Sun-Synchronous orbit at a mean altitude of 817 km. Note that the Sentinel-6A coverage changes over time while it is fixed for the Metop satellites. Furthermore, there are a number of linear features in the Sentinel-6A coverage, which are mostly GLONASS occultations, resulting from the similar inclination of the orbit planes occupied by the Russian constellation (about $65°$).

The Sentinel-6A satellite, showcased by a 1:1 scale model at the EUMETSAT entrance as depicted in figure 2, is equipped with a suite of instruments primarily designed to support the functionality of the Poseidon radar altimeter, its principal payload. Notably, the Radio Occultation (RO) experiment aboard S6A is considered a mission of opportunity, offering substantial benefits for numerical weather prediction (NWP) models and climate studies at a relatively minimal cost, as discussed in Harnisch et al. (2013) and Cardinali and Healy (2014).

The TriG GNSS-RO instrument, engineered by NASA/JPL and cited in works by Tien et al. (2010), Esterhuizen et al. (2009) and (Ho et al., 2020), tracks in Open-Loop mode a variety of signals: the traditional L1CA and L2 Codeless signals, the newer L2C signal from GPS, and the GLONASS Frequency Division Multiple Access (FDMA) signals on both L1 and L2 bands. The instrument's antenna configuration is optimized for data collection: the forward-looking antenna is arranged in a 3x2 array, while the aft-looking antenna has a 3x4 array, providing higher antenna gain for setting occultations, a factor contributing to

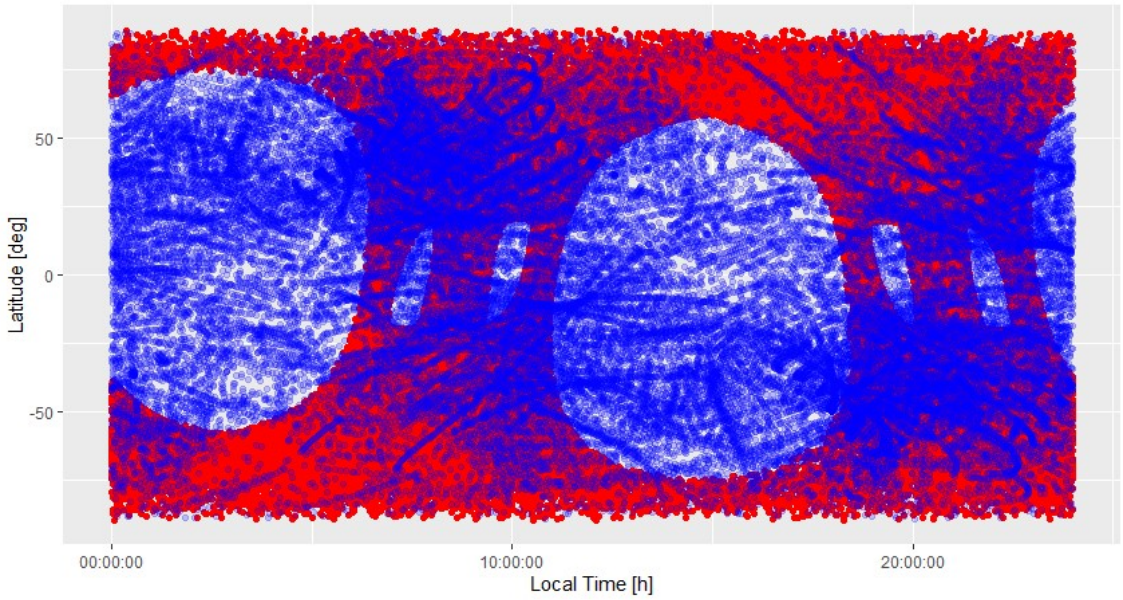

Figure 1. Local solar time coverage for Sentinel-6A (blue) and Metop-A/B/C (red) for October and November 2021.

the discrepancy in the number of setting versus rising occultations. Additionally, the zenith-looking antenna, a single-patch antenna, is dedicated to tracking GPS satellites for precise orbit determination. In a similar way, the COSMIC-2 mission also utilizes the same receiver technology. Indeed, the COSMIC-2 satellites are equipped with the same TriG GNSS-RO instrument, having the same tracking capabilities as Sentinel-6A.

The Sentinel-6A RO instrument requirement is to provide at least 770 quality checked profiles per day. The health of the GNSS constellations significantly affects the number and quality of RO profiles. While the GPS constellation maintains robust performance with more than 30 satellites, the GLONASS system has shown reduced reliability due to aging satellites and slow replenishment rates. To mitigate the impact of GLONASS degradation and enhance overall data collection, there are plans to enable the Sentinel-6A instrument to track Galileo L1/L5 signals, which will increase the quantity and quality of occultation data. The experience from the Sentinel-6A mission emphasizes the importance of having a multi-constellation tracking strategy. This is important in order to ensure the continuous and reliable acquisition of radio occultation data for weather forecasting and climate assessments.

2.1 Data and processing

The Sentinel-6A GNSS-RO dataset, utilized in this paper, spans from September 1st to December 31st 2021, and was sourced from the Sentinel-6A RO-NTC operational processor, which code is based on the Yet Another Radio Occultation Software (YAROS), a EUMETSAT developed and maintained RO processor. It employs the Canonical Transform 2 (CT2) (Gorbunov and Lauritsen, 2004) to deduce bending angles from the complex field measurements along the trajectory of the LEO satellite.

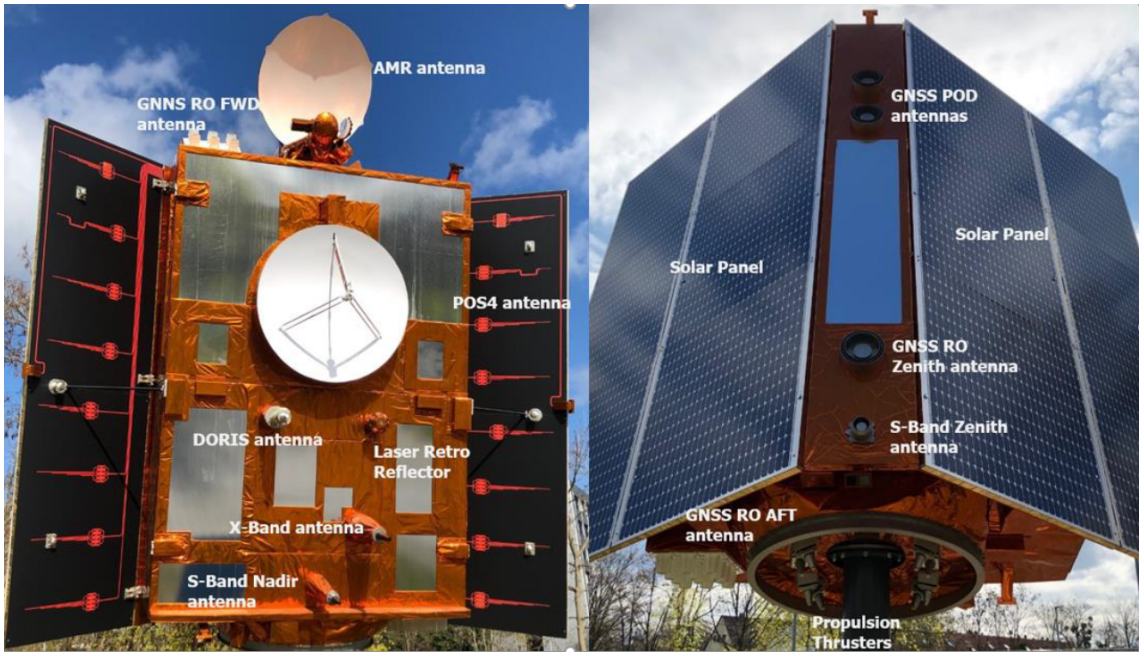

Figure 2. Picture of the 1:1 model of the Sentinel-6A satellite on display on the EUMETSAT campus (von Engeln, 2024). Left: nadir-looking side. Right: zenith-looking side. The main elements are labelled.

As detailed in von Engeln (2022c), prior to calculating bending angles, the Sentinel-6 TriG receiver raw measurements are subjected to a preliminary data reconstruction step, made by using the JPL provided L0 decoder software. This provides files containing occultation radio occultation data together with RINEX-3 files containing zenith antenna data. Subsequent reconstruction and calibration steps include signals SNR and phase reconstruction, Precise Orbit Determination (POD) using the Bernese GNSS Software v5.3 (Dach et al., 2015) developed by the Astronomical Institute of the University of Bern (AIUB), measurement times and signals phase corrections to remove receiver and transmitter clock bias and removal of navigation bits by using NASA/JPL provided navigation bit files. Notably, navigation bit removal is mandatory for L1 in GPS and for both L1 and L2 in GLONASS signals. As outlined in section 2.1.5, the GPS L2P signal necessitates a distinct process to eliminate half cycle slips from the raw phase. Bending angle profiles, stored into level 1B products which format is specified in von Engeln (2022b), are available at the EUMETSAT website https://navigator.eumetsat.int/start.

To ensure the generation of high-quality and reliable POD solutions, NASA/JPL has activated the provision of essential auxiliary data. This includes GPS and GLONASS orbits and clock bias files, Earth Orientation Parameters (EOP) files, and LEO/GNSS attitude data files. The GPS and GLONASS orbital data are updated every 15 minutes, while GPS clock biases are provided at 30-second intervals. Notably, GLONASS clock biases are supplied at a more frequent 1-second rate, a critical factor for enhancing the quality of bending angle products derived from GLONASS occultations (Padovan et al., 2024). For a

Time	Description
01/09/2021 05:01:30	Yaw Flip Backward Configuration
03/09/2021 05:07	Data gap, duration 113 min
05/09/2021 06:33:00	Yaw Flip Forward Configuration
09/09/2021 13:22	Data gap, duration 45 min
08/10/2021 09:41	Data gap, duration 60 min
19/10/2021 07:59	Data gap, duration 52 min
25/10/2021 08:18	Data gap, duration 37 min
05/11/2021 16:18	Data gap, duration 34 min
05/11/2021 16:24:28	Yaw Flip Backward Configuration
09/11/2021 17:28:38	Yaw Flip Forward Configuration
16/11/2021 11:00	Data gap, duration 32 min
16/11/2021 11:03:40	GNSS-RO Script Update Start Period
16/11/2021 11:23:01	GNSS-RO Script Update End Period
25/11/2021 16:48	Data gap, duration 70 min
26/12/2021 17:00	Data gap, duration 63 min
28/12/2021 19:15	Data gap, duration 30 min
30/12/2021 15:29	Data gap, duration 35 min

Table 1. GNSS-RO instrument activities performed between September and December 2021.

detailed list of the auxiliary data files received by NASA/JPL and the ones generated by the Sentinel-6A RO-NTC processor, available on the EUMETSAT website, please consult von Engeln (2022a).

Throughout the period under study including commissioning and early operational phase, routine operations and specific instrument activities were conducted, some of which influenced the daily count of produced occultations and the overall data quality. Table 1 details the instrument-related events and issues that impacted the RO data during this time frame, for the periods where occultations were not recorded for duration exceeding 30 minutes. For a more exhaustive description of instrument activities recorder since the beginning of the mission, refer to von Engeln (2024).

The validation process involved comparing the statistics of two operational RO missions: the 2 Metop B/C satellites with their GNSS Receiver for Atmospheric Sounding (GRAS) instruments, providing about 700 occultations per day each, and SPIRE, which operates a fleet of 3U cubesats (https://spire.com/spirepedia/cubesat/), equipped with the STRATOS GNSS RO instruments. SPIRE occultations are observed by a diverse fleet of satellites operating in both high inclination, near-polar orbits and low inclination, equatorial orbits. This strategic deployment improves data coverage in terms of latitude and longitude, as well as improving temporal coverage in terms of local time. These statistics were benchmarked against operational short-range forecasts from the European Centre for Medium-Range Weather Forecasts (ECMWF). For both datasets, bending angle profiles were thinned to the common set of 247 vertical levels, as for the near-real time disseminated BUFR products as used by

Numerical Weather Prediction (NWP) centers. Metop-B and Metop-C occultations, available through the EUMETSAT ground segment, were analyzed for the specified period. In the case of SPIRE, four satellites were selected to generate statistics to ensure a comparable number of occultations with Metop and Sentinel-6.

The generation of bending angle statistics against ECMWF data involves co-locating profiles on a $0.5\,\mathrm{deg}$ grid resolution and applying 1D forward modeling using the RO Processing Package (ROPP). This process begins by interpolating ECMWF's temperature, humidity, surface pressure, and surface geopotential data to the reference location in a bi-linear fashion as described in (Consortium, 2021). These interpolated data, provided at 137 vertical levels, are then used to derive model-equivalent bending angles at 247 levels. The forward-modeling process employs the Abel integral, which takes the refractive index (derived from ECMWF data on temperature, humidity, and pressure) and computes the bending angles to the common 247 levels.

To demonstrate the enhancements in the Sentinel-6A RO-NTC processor software during the satellite commissioning phase, which started after the satellite launch and concluded on November 19^{th}, 2021, an additional validation was conducted using reprocessed bending angles from Sentinel-6A. This reprocessing used the latest Sentinel-6A RO-NTC processor version 4.0, scheduled for operational deployment in the second quarter of 2024. Reprocessing was also applied to EPS and SPIRE data to maintain consistency across the datasets for comparison.

2.1.1 Daily occultations

Figure 3 displays the daily count of quality checked bending angle profiles processed by the operational EUMETSAT Sentinel-6A RO-NTC processor during the analyzed period, categorized by GNSS system. The black bars represent the combined total number of daily GPS and GLONASS occultations, and the black horizontal line marks the mission's target of 770 bending angle profiles per day. To fully understand this figure, it should be examined alongside Table 1, which enumerates the activities carried out on the S6A satellite and the RO instrument. These activities have had an impact on the RO processing during commissioning and early operational phase, and their inclusion in the analysis helps to contextualize the fluctuation in the number of daily occultations, providing a comprehensive view of operational performance and any external factor affecting it.

Due to the three GLONASS orbit planes, the instrument exhibits fluctuations attributable to the changing visibility of satellites from the Low Earth Orbit (LEO) plane. These variations are a result of the limited number of GLONASS orbit planes, which affects the satellite visibility and, consequently, the number of occultations recorded. Conversely, the six GPS orbit planes provide a more stable and consistent satellite visibility from the LEO perspective, leading to less variation in the daily count of GPS occultations. This stability inherent in the GPS system ensures a more uniform distribution of occultations over time.

The first significant decrease in the number of daily processed occultations was observed on September 2^{nd} and 3^{rd}, 2021. During this period, the RO-NTC processor was unable to process GLONASS occultations because of missing data in the GNSS orbit files provided by JPL. This lack of data led to gaps in the processing capability of the RO-NTC system, specifically affecting the handling of GLONASS signals and resulting in a noticeable reduction in the total number of occultations processed during these days. Subsequent Sentinel-6A RO-NTC processor updates made it more robust to this kind of issues.

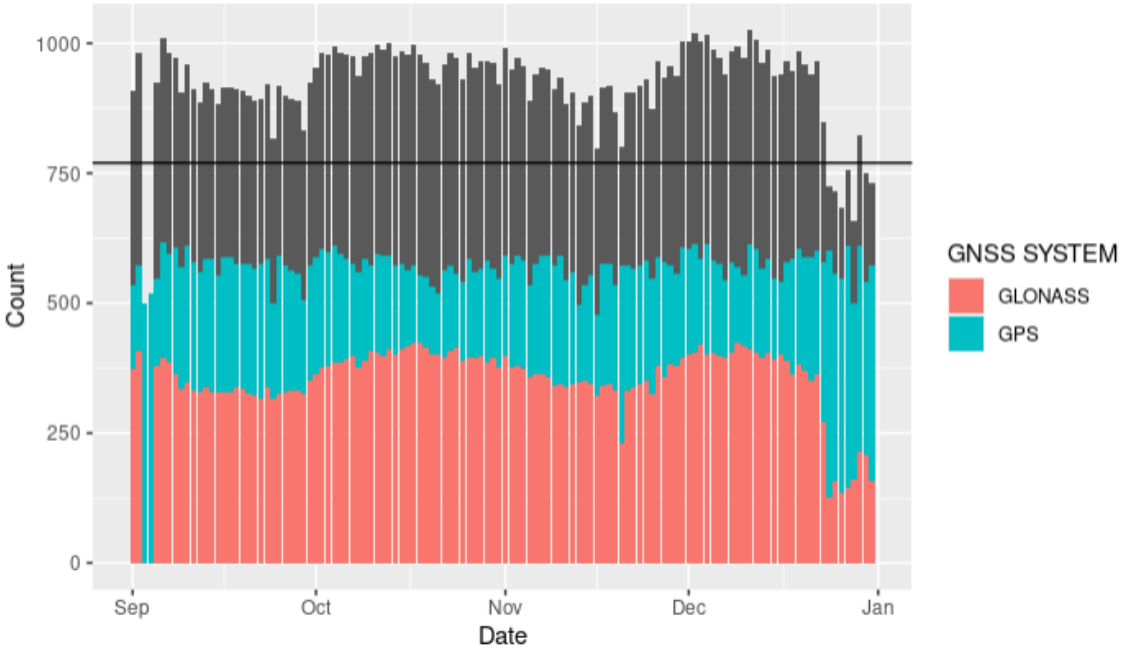

Figure 3. Daily number of quality checked bending angles profiles per constellation in the analyzed period. The black bars indicate the sum of daily GPS and GLONASS occultation profiles, while the black horizontal line indicates the mission requirement of 770 occ/day.

On December 23rd, 2021, another significant reduction in daily occultations was recorded when the GNSS-RO instrument stopped tracking occultations from the GLONASS constellation with satellite numbers greater than 06. This issue led to a decrease of approximately 50% in the total number of GLONASS occultations, persisting until January 2nd, when the instrument was reset. Although not depicted in Figure 3, post-reset, the instrument functioned normally until January 8th, when the problem recurred. A subsequent instrument reboot temporarily addressed the issue, but it was not until a series of software updates between January 12th and 13th, 2022, that the problem was definitively resolved. Further investigations into the cause of the issue revealed that the instrument's malfunction was due to the use of stored, outdated, and no longer updated GLONASS ephemerides, which impacted its proper operation.

Minor decreases in daily occultations were noted during updates to the instrument's configuration for handling yaw flips. During these maneuvers, the satellite is rotated 180 degrees, causing the antenna that normally tracks setting occultations to track rising occultations, and vice versa. These yaw flip phases, which typically last less than 10 minutes, can lead to degraded or unavailable occultations. The brief duration of these flips means that their impact on the total daily occultations is limited, but they can still cause noticeable fluctuations in the data during the periods when the satellite is reorienting itself.

Minor reductions in daily occultations can also result from data gaps in the raw level 0 data provided by the RO instrument. These gaps may arise from various causes, including autonomous or commanded instrument reboots, updates to the instrument's software, downtimes in the data link, or any other incidents leading to the loss of level 0 data. Regarding reboots,

they can occur for the whole instrument or for the science processor only. An instrument reboot leads to a downtime of the instrument and no data is collected. A science processor or software reboot leads to a downtime of that specific processor. Instrument software updates executed prior to the analyzed period enhanced the system's autonomous monitoring capabilities. These updates allow the instrument to initiate automatic science processor reboot commands whenever issues are detected in the occultation data. A significant problem during the early mission phase was the occasional loss of all GLONASS data for extended periods, as occurred on December 23rd, 2021. Initially, such problems required manual processor reboots, but with the updated software, these reboots are now handled autonomously, ensuring more consistent data collection and system stability. Currently the instrument science processor reboots once per day to remove any corrupted data. These reboots don't generally lead to longer losses of any occultation data.

2.1.2 SNR analysis

The analysis of the SNR of the GNSS signals tracked by the RO instrument is an important aspect of radio occultation retrievals. As discussed in the works of Gorbunov et al. (2022a) and Gorbunov et al. (2022b), higher SNRs improve the tropospheric penetration of RO profiles. The effect of SNR to the random error when RO profiles are compared against NWP data is mission dependent, showing some saturation features larger for some missions and smaller for others. It´s worth nothing that lower SNR missions like SPIRE have demonstrated the ability to systematically detect critical atmospheric features, particularly in the lower troposphere (Ho et al., 2023). In this section, we aim to delineate the SNR characteristics specific to the Sentinel-6 RO receiver, contributing with its good performance to the field of atmospheric observations.

The histograms in Figure 4 display the distribution of Sentinel-6A mean SNRs, highlighting that GLONASS signals exhibit higher SNRs compared to GPS signals, attributed to the not required code-less tracking for GLONASS. To fully understand the SNR distributions, Figure 4 should be analyzed in conjunction with Figures 5 and 6. Figure 5 presents the mean SNRs plotted per satellite number, averaged over the analyzed period, and categorized by constellation and frequency. Figure 6 shows the daily averages of mean SNRs, grouped according to the tracked GNSS signal code. The GPS distributions show lower SNRs compared to GLONASS, more visible for the L2 plot. The different gains of the rising and setting antennas are slightly more pronounced for L1 plot than for L2 plot, peaking at about 1250 V/V and about 1000 V/V, as also noticeable in the GPS-related panels of Figure 6.

In contrast, the SNR distributions in Figure 4 for GLONASS are tri-modal for both L1 and L2 frequencies. Notably, peaks in L1 around 500 V/V are influenced by satellites R13, R19, R20, and R22, as seen in the bottom left panel of Figure 5. Additionally, for L1, there are peaks at approximately 1000 V/V and 1700 V/V, while for L2, the peaks are at around 300 V/V, 750 V/V, and 1250 V/V, influenced by satellites R13, R16, and R22 as seen in the bottom right panel of Figure 5.

The analysis of GPS signals per satellite number, as shown in Figure 5, indicates that while some satellites perform better than others, the SNRs and tracking capabilities of GPS signals remain relatively stable across different satellites. This consistency applies to both L1 and L2 GPS signals, with no significant distinction observed between the tracking of L2P and L2C signals, a finding confirmed by the top right and bottom left panels of Figure 5.

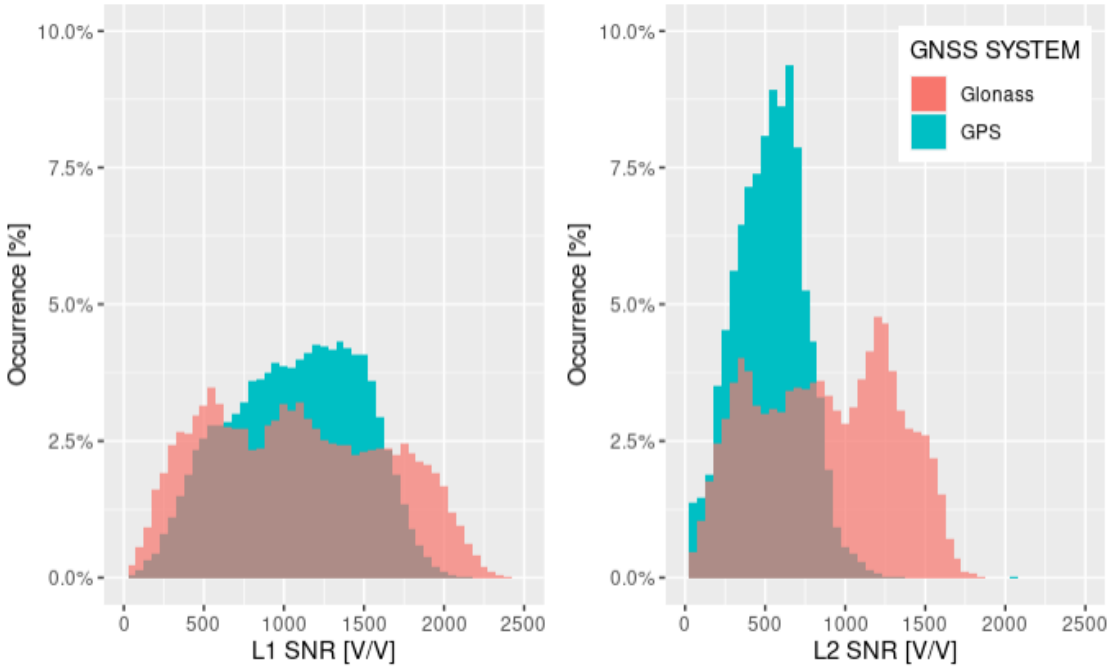

Figure 4. Histograms of mean SNRs measured between 60 and 80 km Straight Line Tangent Altitude (SLTA) split per constellation, for L1 (left) and L2 (right) frequencies.

In contrast, GLONASS exhibits more variability in SNR values among its satellites. Specifically, L1 is tracked with an SNR lower than 500 V/V for satellites R13, R19, R20, and R22, and L2 shows similar SNR values for satellites R13, R16, and R22. Notably, for satellites R13, R19, and R20, the SNRs are more favorable for L2 than for L1. This variation in GLONASS SNRs indicates a disparity in signal strength and tracking efficiency across its constellation, contrasting with the more uniform performance observed in the GPS system.

The further examination of mean observed SNRs involves daily average calculations, segmented by tracked signal and differentiated between setting and rising occultations. These results are depicted in Figure 6. The time series in this figure illustrates the impact of yaw flips executed in early September and November, particularly when not followed by beam forming adjustments. In such cases, the beam forming that was initially optimized for the rising and setting antennas becomes misaligned once the antennas are switched, leading to a significant reduction in SNR. It´s worth noting, comparing Figure 4 with Figure 6 that, during yaw flips the tracking capabilities remained unchanged. This is confirmed by the yaw flip event that occurred between November 5^{th} and 9^{th} 2021. The yaw flip in early September also demonstrates the robust tracking abilities, although one has to exclude September 2^{nd} and 3^{rd}. On these days, the absence of GNSS orbit files from JPL resulted in the processor's inability to process GLONASS occultations as reported in Section 2.1.1.

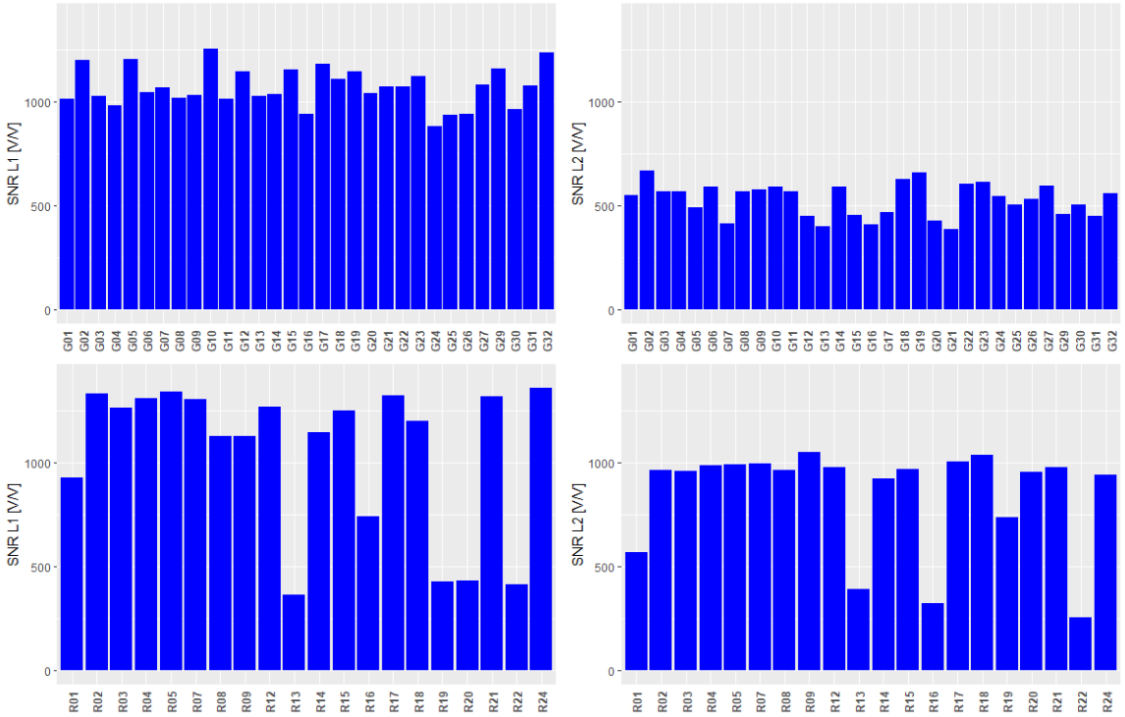

Figure 5. Mean SNRs measured between 60 and 80 km SLTA, plotted by satellite number and averaged over the analyzed period. The data is split by GPS (top) and GLONASS (bottom), as well as by L1 (left) and L2 (right) frequencies.

Moreover, Figure 6 highlights the variability in tracking capabilities for GLONASS signals over time, which is influenced by the geometrical configuration of the orbits. This variability contrasts with the more stable tracking performance of GPS signals, underscoring the sensitivity of GLONASS tracking to its orbital geometry. Such temporal fluctuations in SNR for GLONASS signals emphasize the dynamic nature of satellite tracking performance and the importance of considering orbital geometries in the analysis of GNSS data quality.

To provide a thorough assessment of the Sentinel-6A TRIG RO instrument, it is essential to examine not only the SNR values but also the phase noise impacting the tracking of GNSS signals (Withers, 2010). Phase noise represents the random variations in the phase of the tracked signals, arising from different sources, including electronic components or imperfections in the receiver. This noise can distort the received signal, leading to inaccuracies in the estimation of phase delays induced by the atmosphere.

High phase noise can negatively affect the SNR by adding random fluctuations to the received signal. Conversely, a low SNR can make the tracking more vulnerable to phase noise, highlighting the interdependent nature of these two parameters. Major contributors to the bending angle error budget in the upper stratosphere include phase noise as well as the the Precise Orbit Determination (POD) solution (Padovan et al., 2024) and residual ionospheric errors (Gorbunov, 2002; Danzer et al., 2013, 2015; Healy and Culverwell, 2015) remaining after the ionospheric contribution correction. Figure 7 shows the histograms of the

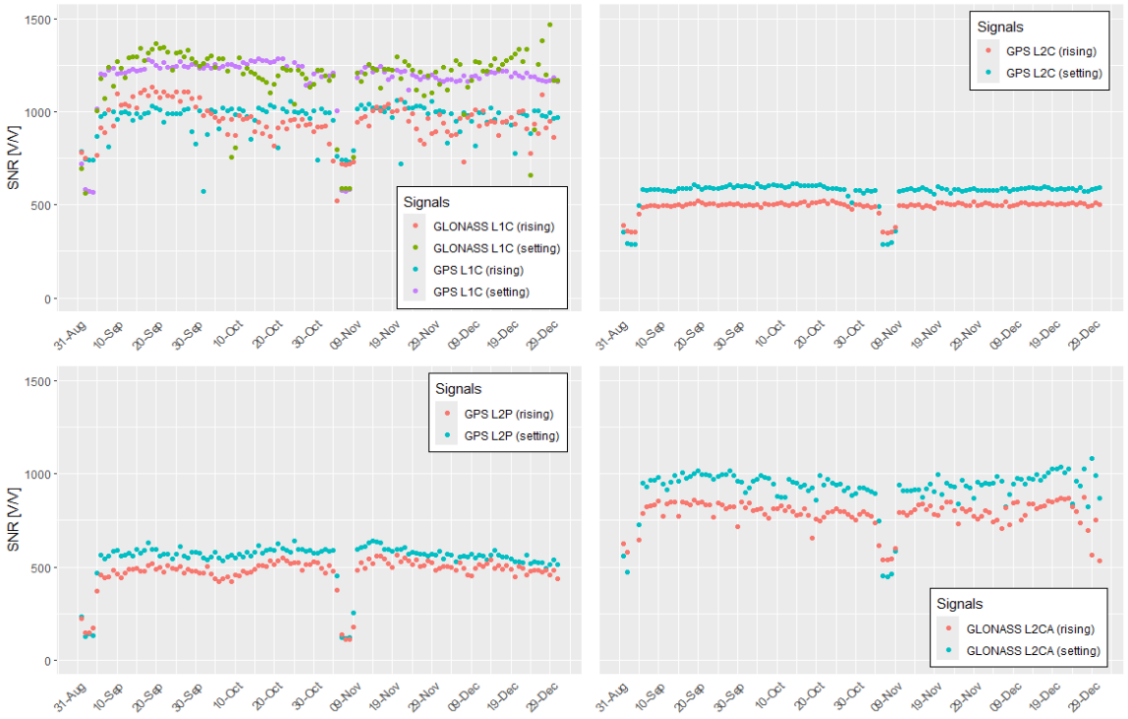

Figure 6. Daily average mean SNRs measured between 60 and 80 km SLTA, categorized by GNSS signal code and split between rising and setting occultations. The top left panel shows values for GPS and GLONASS L1C codes, while the top right, bottom left, and bottom right panels report SNR values for GPS L2C, GPS L2P, and GLONASS L2CA codes, respectively.

excess phase noise distribution for L1 and L2, calculated per occultation between 60 and 80 km SLTA. This figure reveals that the RO instrument experiences lower phase noise levels when tracking GLONASS occultations compared to GPS ones.

In comparison to the other two missions discussed in this paper, Sentinel-6A exhibits phase noise levels that are slightly higher than those of the GRAS instrument, with an average around 0.08 mm. However, these levels are significantly lower than those of SPIRE, where the phase noise typically ranges between 0.5 mm and 1.3 mm. This comparison highlights the relative performance of Sentinel-6A in terms of phase noise, situating it between the lower noise levels of GRAS and the higher levels associated with SPIRE. The data suggests that Sentinel-6A maintains a good balance in phase noise performance, offering a more favorable operational condition for atmospheric sounding compared to SPIRE, while slightly lagging behind the performance of GRAS.

2.1.3 L1/L2 signals cut-off based on SNR

Over the past decade, the tracking capabilities of GNSS receivers used for positioning purposes have significantly improved, and RO GNSS receivers are not excluded (Gill et al., 2023). In particular, the Open-Loop tracking mode represents a major evolution of the tracking function (Mohamady and Amiri, 2013; Tien et al., 2010; Ao et al., 2009). This mode leverages on

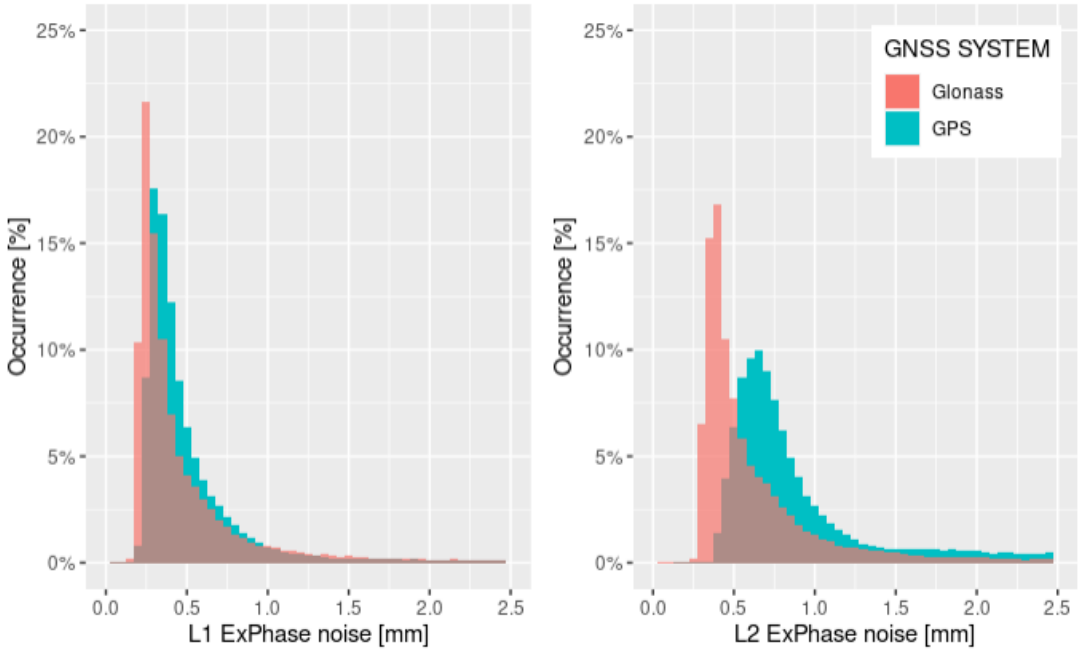

Figure 7. Histograms of Excess Phase noise measured between 60 and 80 km SLTA split per constellation, for L1 (left) and L2 (right) frequencies.

a priori knowledge (model) of the atmospheric delay, or equivalently, the atmospheric Doppler, which the receiver uses to initially estimate the received GNSS signal frequencies.

The introduction of Open-Loop tracking in RO receivers has notably enhanced their tracking capabilities, especially in the moist lower troposphere, where Closed-loop tracking mode encounters problem related to the Phase-Locked Loop (PLL) tracking technique. Open-Loop tracking mode facilitates improved tropospheric penetration (Sokolovskiy et al., 2009), enabling more reliable and accurate data collection in these regions. Currently, Open-Loop tracking mode is widely employed in many RO missions, sometimes extending to the middle and upper stratosphere, or even completely replacing the Closed-Loop mode as it is for Sentinel-6 RO receiver.

In Open-Loop tracking mode, an important characteristic of the GNSS signals is the presence of long tails at the lowest SLTA, which are sometimes primarily composed of noise. This is the case of Sentinel-6A RO instrument, set to reach SLTA values down to -350 km. Despite the EUMETSAT RO processor employs the fast phase transform technique to minimize inversion errors in the retrieval of bending angles, inaccuracies may still arise due to the length of the recorded signals and the associated noise. The cut-off height for the L1 and L2 signals can significantly influence the bias structure in the troposphere when occultation profiles are analyzed against reference data, such as ECMWF data (Sokolovskiy et al., 2010). Therefore, the

determination of the appropriate cut-off height becomes critical in ensuring the accuracy and reliability of tropospheric data obtained from GNSS signals in Open-Loop tracking mode.

Modifying the cutoff points in the RO processing for L1 and L2 signals recorded in Open-Loop mode significantly affects the retrieval of bending angles in two ways. Firstly, the RO geometry imposes that rays with larger bending angles will be received later by the receiver, which in turns means that they will be received at lower altitudes. If the signal cutoff is set too high, these late-arriving rays at lower altitudes will be excluded from the signal processing, potentially leading to an underestimation of bending angles at these heights. This could result in a more negative bias in the tropospheric bending angle profile when compared with ECMWF data, an effect that is particularly pronounced in lower latitude bands where the troposphere contains more moisture.

Secondly, lowering the signal cutoff point too much might allow the inclusion of mostly noise (noise tail) in the bending angle processing, introducing a positive bias. Thus, finding the optimal cutoff point is a delicate balance: it must be high enough to exclude noise but low enough to capture the complete signal, especially in regions with high moisture content.

The Sentinel-6 RO processor employs the SNR-based signal cutoff algorithm for L1 and L2 signals, as detailed in Sokolovskiy et al. (2010), with minor modifications to address the zero amplitude/SNR occurrences regularly noted in L2 data from JPL receivers. Figure 8 demonstrates the impact of this implementation on the bias structure within the tropospheric heights, revealing a shift of about 1% to the right when the data are compared against ECMWF.

2.1.4 L2 signals cutoff and L2 extrapolation in troposphere

After the launch of the Sentinel-6A satellite, during its commissioning phase and subsequently, investigations were initiated to address issues related to the cut-off of L1/L2 GNSS signals and the extrapolation of the L2 signal performed by the Sentinel-6A RO processor in the troposphere. These investigations were prompted by observations of excessively biased L2 frequency data in the tropospheric segment of some occultations. The Sentinel-6A RO processor follows the ionospheric correction procedure outlined in (Culverwell and Healy, 2015). Given that the L2 signal is more susceptible to SNR reductions, this procedure suggests to cutoff the L2 signal in troposphere, where it becomes noisier, and extrapolate it to lower altitudes using an ionospheric model based on a Chapman Layer. This is done before the L1 and L2 bending angle profiles are merged to eliminate the ionospheric influence. The smooth transition of actual measurements with the extrapolated ionospheric model occurs within a transition range, commencing from the L2 cutoff point and progressively blending into the real measurements. The determination of the L2 cutoff point was a significant focus of this investigation, aiming to enhance the accuracy and reliability of the RO tropospheric data processed by the Sentinel-6A RO processor.

The initial approach for processing the Sentinel-6A RO data involved using a fixed threshold of 50μrad to determine the cutoff point for the L2 signal based on the L1-L2 bending angles difference. This method significantly improved the bending angles processing, as indicated in Figure 9, showing the effect of enabling and disabling the L2 signal cutoff algorithm. However, it encountered issues during periods of high solar activity, where increased variability and a negative bias in the L1-L2 bending angle residuals often resulted in the L2 signal being truncated prematurely at too high an altitude. To counter this, a conservative height threshold of 30km was set to prevent the L2 signal from being cut above this altitude.

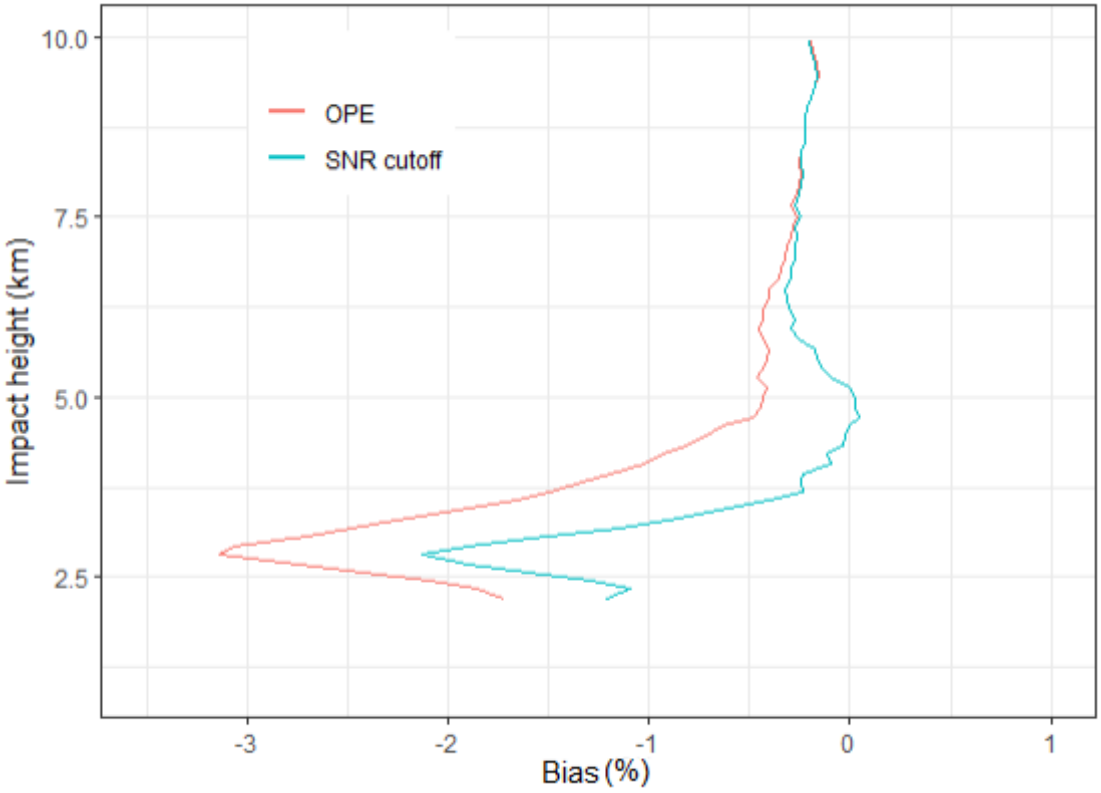

Figure 8. Global robust statistics of S6 bending angles compared against ECMWF short range forecasts during the analyzed period. Only vertical profiles of biases (or systematic deviations) in troposphere are shown for operational and reprocessed data employing the SNR-based cutoff algorithm.

Figure 10 presents the density distribution of the L1-L2 difference for two distinct dates, December 10^{th}, 2021 (a period of low solar activity) and December 23^{rd}, 2021 (a period of high solar activity), at various altitudes. Under the 50μrad threshold with a maximum cut-off height of 30km, the L1-L2/L2 signals are typically truncated above 5km during low solar activity periods, with the cut-off occurring slightly higher during periods of high solar activity.

As observed and previously mentioned, employing a fixed threshold for the L2 signal cut-off, as depicted in Figure 10, can result in prematurely cutting the L2 signal, especially under varying solar activity conditions. To address this, an enhanced implementation, which is now operational, adopts a robust mean of the L1-L2 bending angles as the reference point for applying the 50μrad threshold to determine the L2 cut-off. This adjustment is made before the ionospheric correction process, enabling a more dynamic response to fluctuations in the L1-L2 bias induced by different levels of solar activity. This method allows for a more accurate representation of the ionospheric impact on the L2 signal, ensuring that the cut-off is applied more appropriately across varying solar conditions.

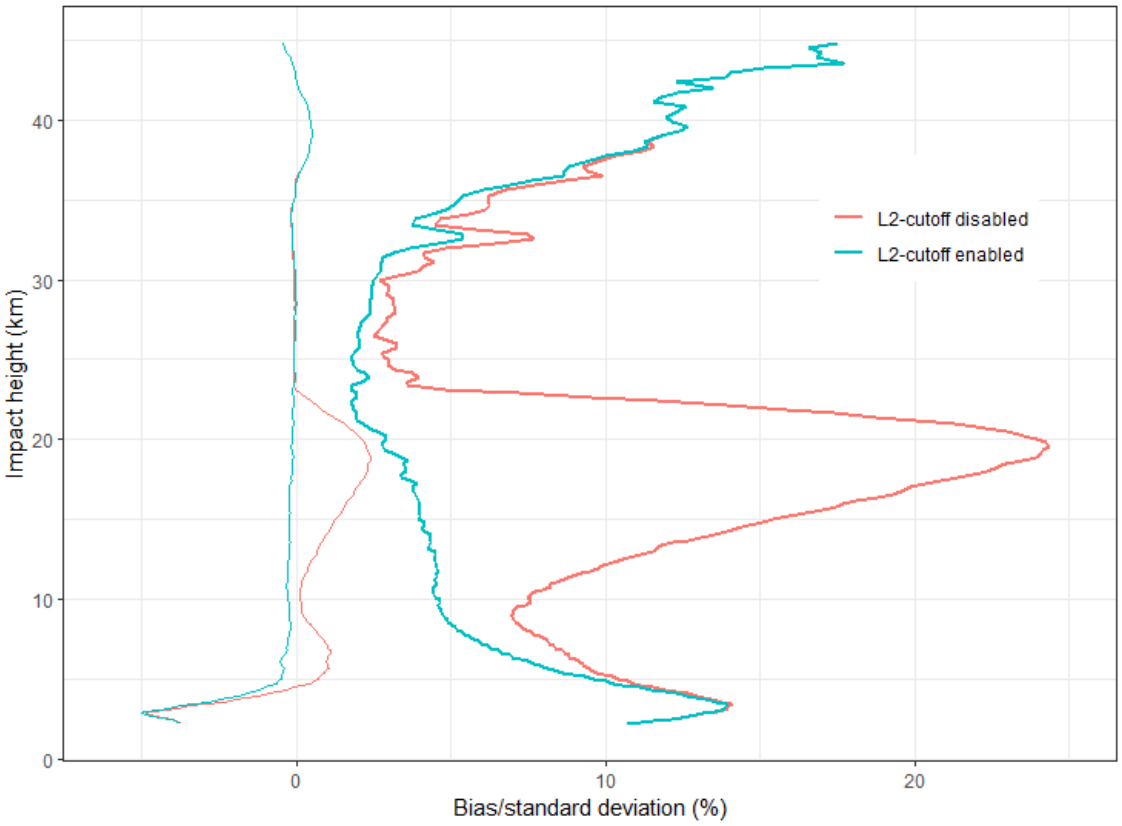

Figure 9. Global normal statistics of S6 bending angles compared against ECMWF short range forecasts during December 2021. The vertical profiles of biases (or systematic deviations) with thin lines and respective standard deviations (or random deviations) with thick lines are shown for two runs: one with the L2 signal cutoff algorithm activated (red) and one without it (blue).

An alternative approach consists of integrating the L2 cutoff into the bending angles ionospheric correction process. This involves using a robustly fitted ionospheric model to the current data as the reference for determining the L2 signal cutoff point, in line with the suggestions in Culverwell and Healy (2015). Figure 11 presents normal statistical comparisons of bending angles against ECMWF data, showing the performance of a normal (or non-robust) and a robust ionospheric bending angle linear fitting algorithm. The data indicates that using the robust linear fitting algorithm can enhance the standard deviation by up to 2.5% compared to operational data using the robust mean approach, above approximately 18km altitude. Between approximately 22km and 36km, the improvement in using robust fitting over non-robust fitting is modest but still significant to demonstrate the decreased sensitivity to strong ionospheric variations.

This investigation suggests that a robust linear fitting is better suited for handling irregular L1-L2 bending angles and is less impacted by noisy L2 data at lower tropospheric altitudes. Consequently, despite the modest improvement in the ran-

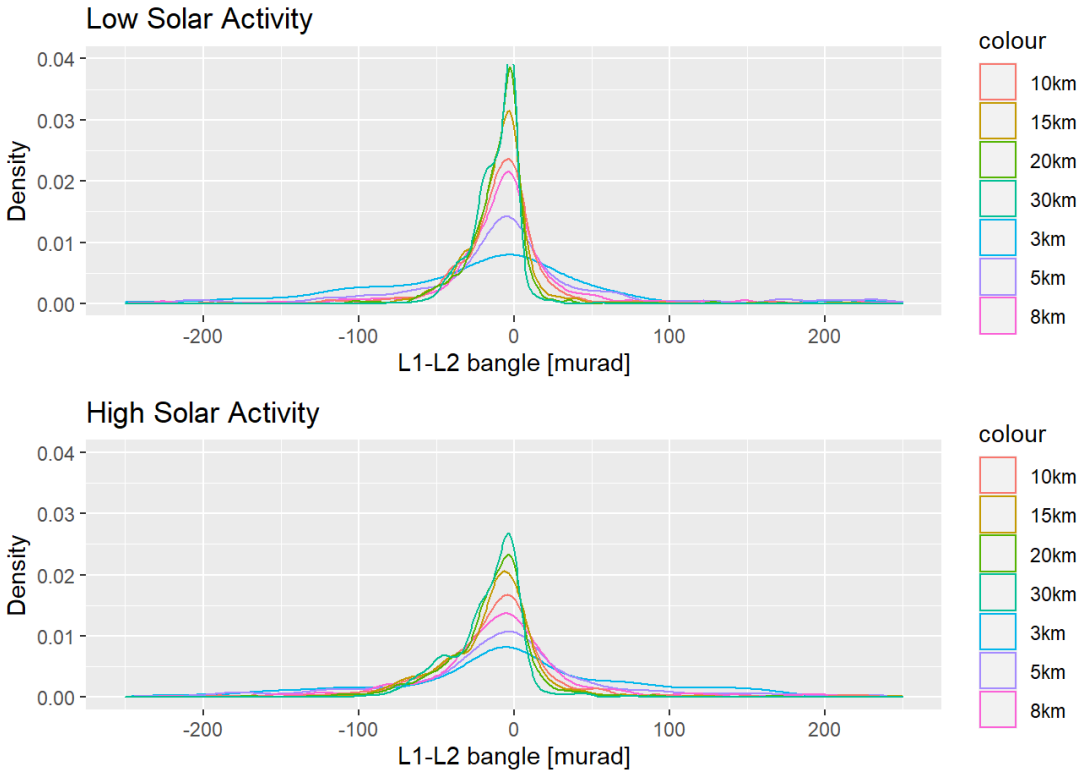

Figure 10. L1-L2 difference density distribution for December 10th 2021 (low solar activity) and December 23rd 2021 (high solar activity) at different heights.

dom error, the robust fitting approach is still favored in presence of strong ionospheric disturbances, making it a worthwhile implementation choice for L2 signal cutoffs in the ionospheric correction phase.

2.1.5 Navigation bits removal

One of the preparatory steps before starting the bending angle retrieval algorithm involves removing navigation bits from the
370 received L1/L2 GNSS signals. In the Sentinel-6 RO-NTC processor, this process makes use of the JPL-provided navigation bits data stream. In the initial version of the Sentinel-6 RO processor, the navigation bits removal using JPL data was followed by an internal half cycle slips detection algorithm applied to all tracked GNSS signals, following the discriminator formulation suggested by Sokolovskiy et al. (2009).

An improved version of the navigation bit removal algorithm adopted by the Sentinel-6 RO processor makes use of the
375 half cycle slips detection algorithm only for the GPS L2P signal, relying on the JPL provided navigation bit data files for the other tracked signals. Figure 12 illustrates the impact of this improved algorithm, displaying the difference in a sample bending angles profile processed by using the revised algorithm and the original version. Noteworthy is the difference between

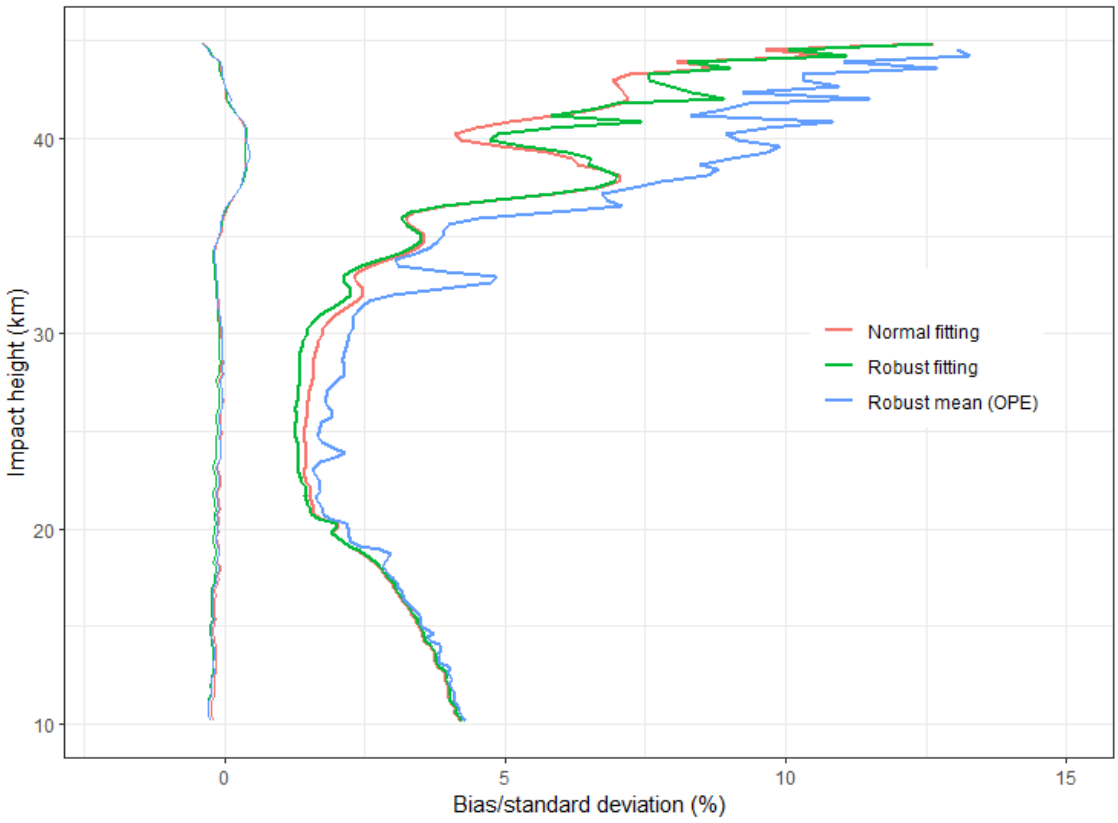

Figure 11. Global normal statistics of S6 bending angles compared against ECMWF short range forecasts during December 2021. The vertical profiles of biases (or systematic deviations) with thin lines and respective standard deviations (or random deviations) are shown for different choices of ionospheric model fitting algorithms.

bending angles in the lower troposphere, where lower SNR signals are tracked and the effects of multi-path processes are most pronounced.

Figure 13 shows the effect to the global bending angle normal statistics resulting from the refinement of the navigation bit removal algorithm, as data are compared against ECMWF models. Improvements to the random error extend from the troposphere between 5k and 23km impact height and to stratosphere above 30km impact height. These modifications have led to an overall enhancement in the quality of the generated bending angle profiles.

2.1.6 Interference on L2 signal

During the commissioning phase of the Sentinel-6A satellite and the routine quality assessment of its RO data, certain occultations revealed the presence of interference signals superimposed on the I and Q components, which were not associated with GNSS navigation bits. Specifically, interference signal at 40/20Hz were detected superimposed on the L2 signals, noticeable

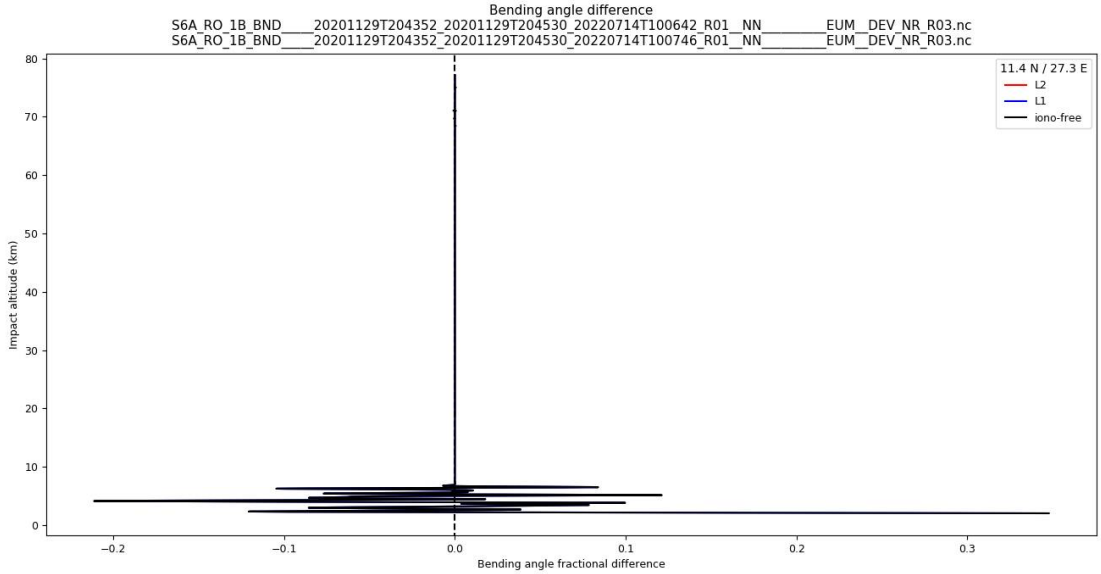

Figure 12. Difference between bending angles of a single occultation profile, retrieved by using the refined version of the navigation bits removal algorithm and the currently operational one.

in the SNR spectrum of these signals. Figure 14 presents the SNR spectrum for both L1 and L2 during a single occultation, highlighting these anomalous frequencies on the L2 plot.

Investigating the origin of interference observed in the SNR spectrum of the L2 signals is an interesting point for assessing its impact on the quality of RO products. Understanding whether these spurious signals are geographically localized is equally important. Figure15 shows the RO receiver's geographical positions for all occultations recorded between August 2021 and May 2022, clearly indicating that these interference are more frequent when the Low Earth Orbit (LEO) satellite passes over the boundary between Russia and America. This observation is in line with findings from Isoz et al. (2014), which examined how terrestrial interference sources influence space-based GNSS receivers, with a specific focus on the GRAS instrument aboard the Metop-A satellite. The study identified that terrestrial interference could induce pulsed interference and background noise fluctuations, without significantly compromising the GRAS data quality. Sentinel-6 data confirm these findings, most likely because the interference does not have enough power to affect the performance of the receiver significantly.

3 Bending angles validation

Figure 16 presents the robust statistics of (O–B)/B, where O (Observable) represents the operational measurements from Sentinel-6A, Spire, and GRAS B/C, and B (Background) is derived from the forward-propagated ECMWF short-range forecasts as a function of impact height. The deviations are expressed in percentage, facilitating a direct comparison of standard deviation values against the magnitudes of actual data at each height level. The data are analyzed using a robust estimator,

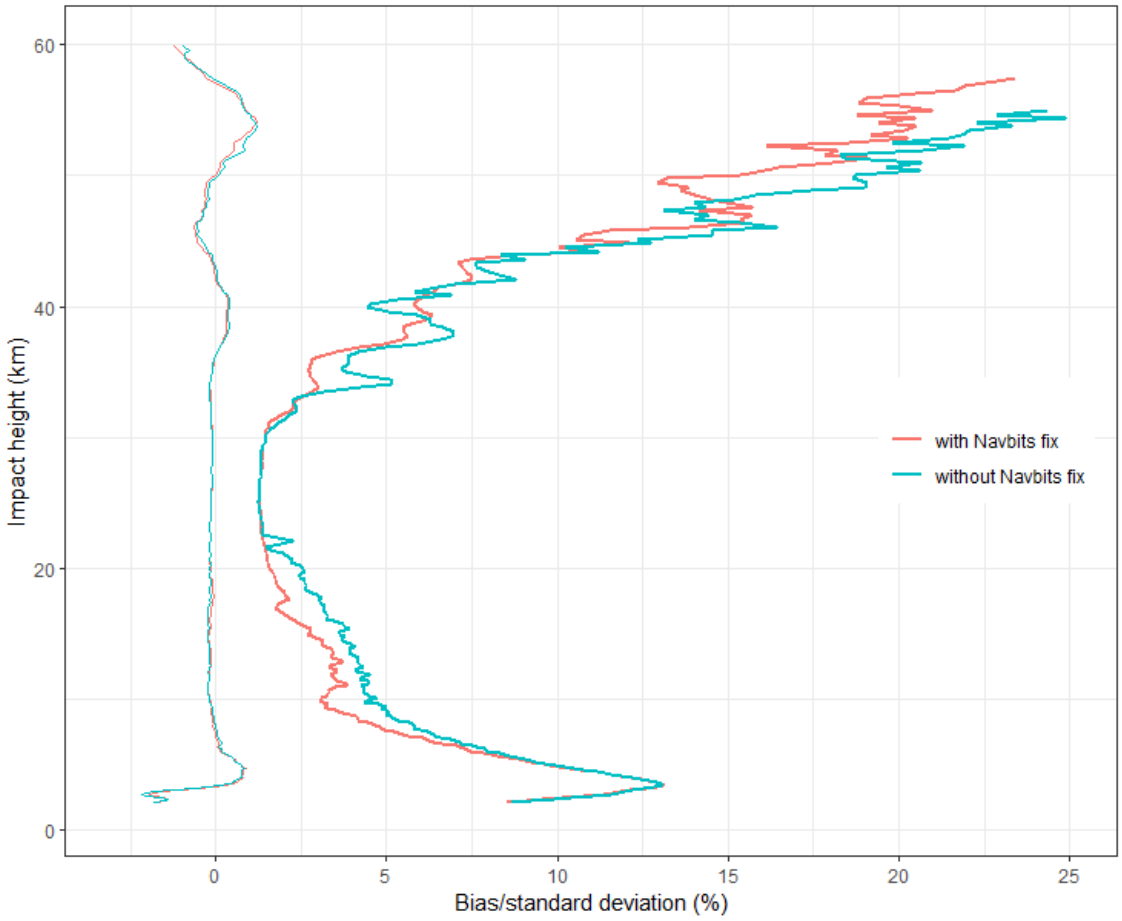

Figure 13. Global normal statistics of Sentinel-6A bending angles compared against ECMWF short range forecasts during the analyzed period. The vertical profiles of biases (or systematic deviations) with thin lines and respective standard deviations (or random deviations) with thick lines are shown for different versions of the RO-NTC processor, with and without the navigation bit removal algorithm refinement. Statistics include both GPS and GLONASS occultations.

as recommended by Hoaglin et al. (2000), which effectively mitigates the influence of outliers in noisy distributions, yielding standard deviation and the percentage of data points within the $\pm 2\sigma$ interval.

The analysis of Figure 16 clearly highlights the high quality of the operational Sentinel-6 bending angles, showing they are largely on par with those from the two EPS missions concerning both systematic and random errors. The standard deviation for Spire's occultations above 30 km is notably higher than that of the other missions, indicating greater data variability from Spire's RO receivers. While some of this discrepancy in the upper stratosphere may be attributed to the POD solution or residual ionospheric errors, the primary cause is the higher signal phase noise levels of Spire measurements, significantly influencing the bending angle error budget at these heights. This finding is supported by the fact that the EUMETSAT RO processor uniformly smooths the bending angles for all missions, hence the inherent phase noise levels in the missions directly impact

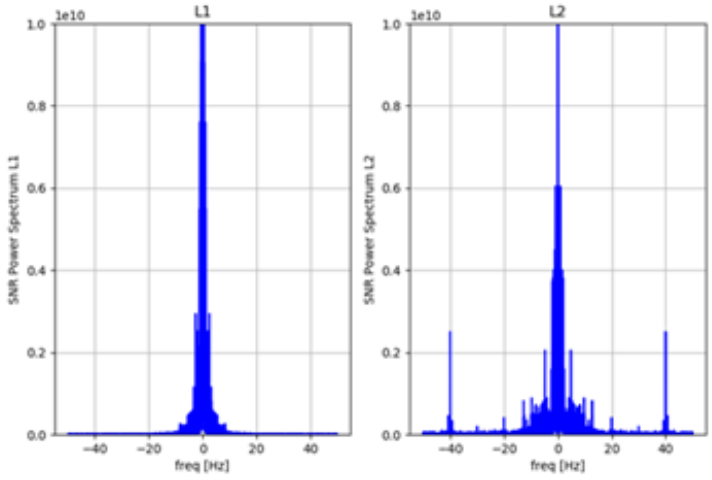

Figure 14. L1 (left) and L2 (right) SNR spectrum for a single Sentinel-6A GPS occultation recorded on October 1st, 2021.

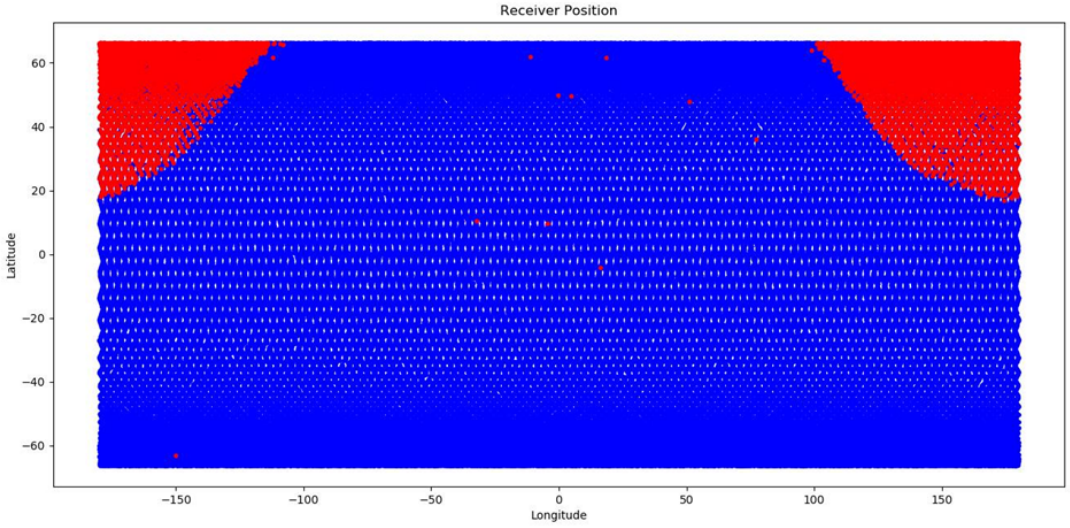

Figure 15. Receiver position for Sentinel-6A occultations affected by the interference signals in the L2 frequency, in the period between August 2021 and May 2022.

the bending angles profiles. The difference in the standard deviation between GRAS or Sentinel-6A and Spire data diminishes towards lower altitudes where other error contributions, in particular horizontal inhomogeneities, become the dominant drivers of RO uncertainty.

Concerning the vertical bias structure, all three missions show high consistency above approximately 7 km impact height (or about 5 km above sea level). Differences emerge in the troposphere, where the distinct instruments and their tracking

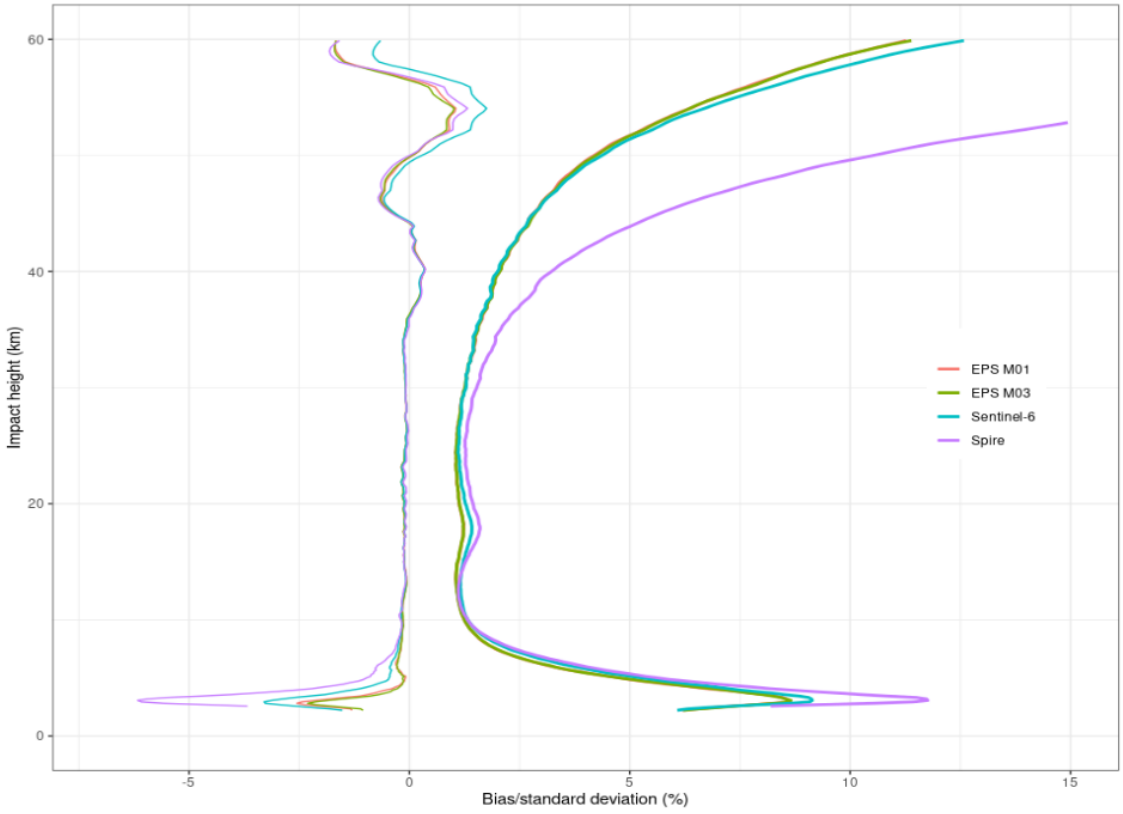

Figure 16. Global robust statistics of operational GRAS (M01/B and M03/C), Spire and Sentinel-6A bending angles compared against ECMWF short range forecasts during the analyzed period. The vertical profiles of biases (or systematic deviations) with thin lines and respective standard deviations (or random deviations) are shown for the different missions.

conditions/modes, alongside the varied signal cut-off strategies, play an important role. Sentinel-6A exhibits a marginally larger negative bias compared to the two EPS missions, yet it is significantly less than that of Spire.

The operational RO data from Sentinel-6A, Spire, and GRAS B/C were reprocessed using the latest version of the EUMETSAT RO processor, set for deployment at the EUMETSAT Sentinel-6A RO-NTC facility in the second quarter of 2024. Figure 17 presents robust statistics from this reprocessing. Slight improvements in the standard deviation for Sentinel-6A are observed around 18km and above 50km, with the data now closely aligning with the GRAS measurements. The enhancement at 18km primarily results from the refined transition between the ionospheric model and actual bending angles measurements, facilitated by the updated L2 extrapolation algorithm in the troposphere (discussed in section 2.1.4). The improvement above 50km comes from the correction made to the Sentinel-6A navigation bits removal algorithm (detailed in section 2.1.5).

An alternative way for inspecting the impact of the navigation bits removal algorithm correction in Sentinel-6A can be examining the bending angles statistics segregated by GNSS system, as depicted in Figure 18. This view highlights a reduction

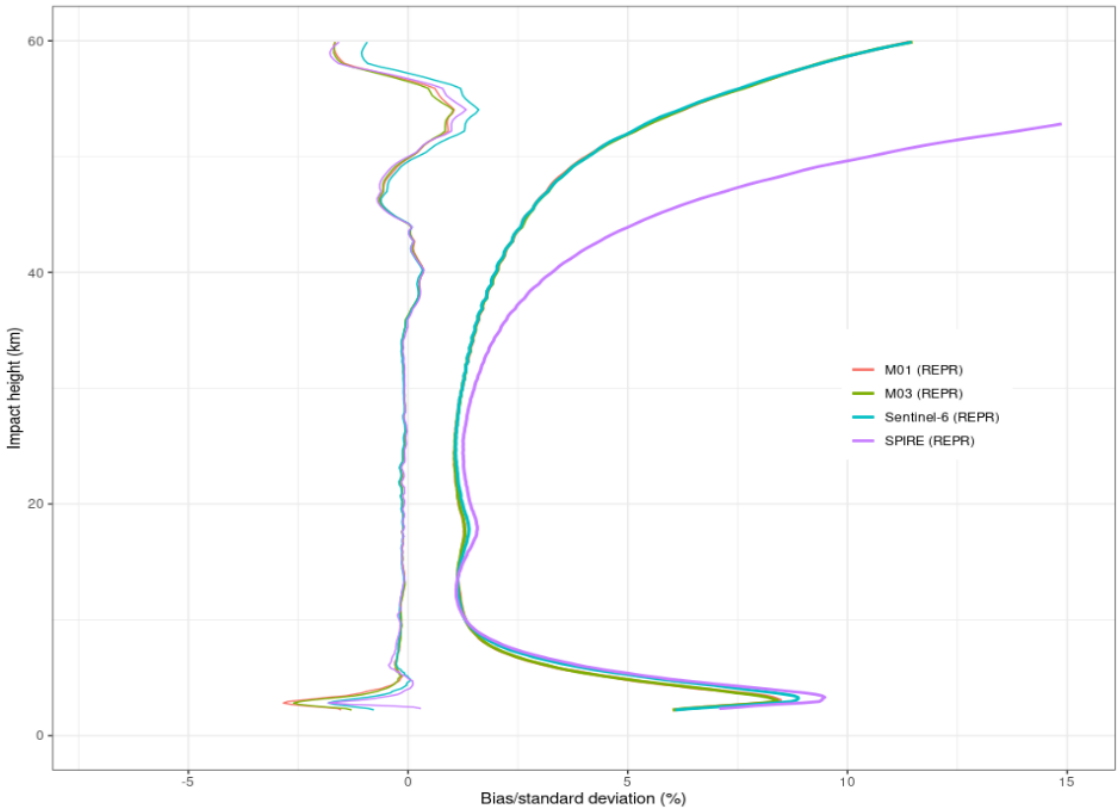

Figure 17. Global robust statistics of reprocessed GRAS (M01/B and M03/C), Spire and Sentinel-6A bending angles compared against ECMWF short range forecasts during the analyzed period. The vertical profiles of biases (or systematic deviations) with thin lines and respective standard deviations (or random deviations) are shown for the different missions.

in the standard deviation for GLONASS occultations compared to GPS occultations, illustrating the specific benefits of the navigation bits removal algorithm's bug fix.

It's noteworthy to say that the GRAS bending angles retrieval algorithm has not yet implemented the SNR-based signal cutoff function (discussed in section 2.1.3), unlike the reprocessed Sentinel-6 and Spire processors. Furthermore, the impact of the L2 cutoff algorithm (referenced in section 2.1.4) is not prominently evident in robust statistics, which are designed to minimize the influence of outliers. Its effects are more discernible in standard statistical analyses that account for the full range of data, including outlier contributions. Consequently, the robust statistics for GRAS depicted in Figures 16 and 17 appear nearly identical, underscoring the need to consider both robust and standard statistical methods to fully capture the effects of the data processing algorithms on RO data quality.

The most significant difference between figures 16 and 17 is observed in the lower troposphere, below 7 km impact height. In this region, the diverse strategies for signal cutoff and extrapolation, as described in Sokolovskiy et al. (2010) and Culverwell and Healy (2015), give their greatest influence. Notably, the substantial negative biases previously seen in the operational

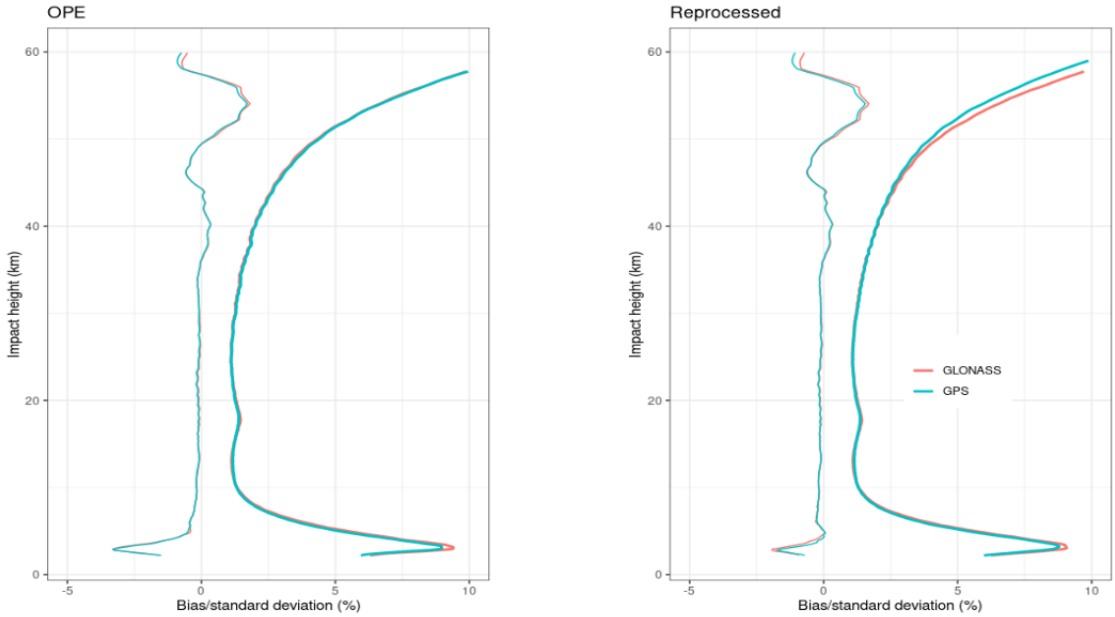

Figure 18. Global robust statistics of operational (left) and reprocessed (right) Sentinel-6A bending angles compared against ECMWF short range forecasts during the analyzed period. The vertical profiles of biases (or systematic deviations) with respective standard deviations (or random deviations) are shown split by constellation.

data from Spire and Sentinel-6A are considerably diminished in the reprocessed data, even surpassing the performance of GRAS B/C data in this region. Figure 19 offers a detailed view of the lower troposphere statistics for both the operational and reprocessed Sentinel-6A data. Beyond the noticeable adjustment in bias structure, the adoption of new cutoff strategies has enabled deeper tropospheric penetration.

The research presented in Sokolovskiy et al. (2010) receives further confirmation from Figure 20, which illustrates how the positive bias in bending angle retrievals primarily depends on the employment and implementation of a signal cut-off algorithm based on SNR, with the cut-off threshold influencing the tropospheric bias. The systematic error biasing effect is less noticeable at higher latitudes, where the troposphere is drier and more stable, thus experiencing less multi-path interference and reduced instances of super refraction. In contrast, at mid-latitudes and especially in the tropics, where the troposphere is thicker and contains more moisture, the influence of signal cut-off becomes more evident, affecting the bending angle measurements down to altitudes below 7 km.

4 Conclusions

The Sentinel-6A Michael Freilich satellite, launched into Low Earth Orbit on November 21st, was primarily tasked with continuing the legacy of the altimetry Sentinel mission series. In addition to its main instrument, the altimeter, it is equipped with

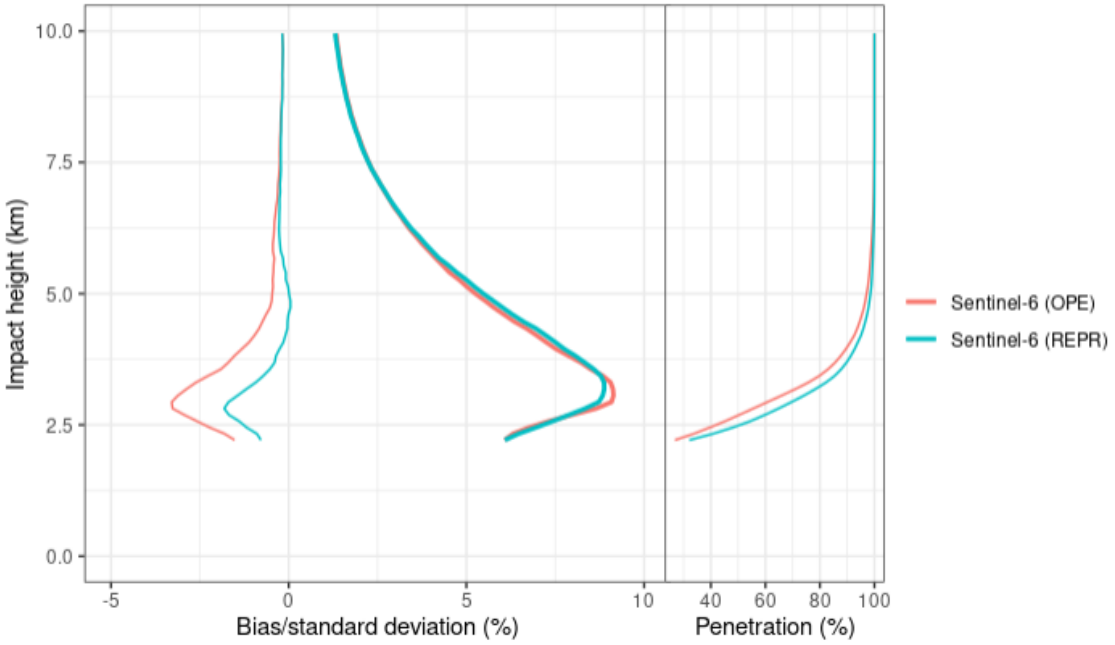

Figure 19. Global robust statistics of tropospheric operational and reprocessed Sentinel-6A bending angles compared against ECMWF short range forecasts during the analyzed period. The vertical profiles of biases (or systematic deviations) with thin lines and respective standard deviations (or random deviations) are shown.

a GNSS RO TRIG receiver. Since its activation, the RO instrument has consistently provided a significant volume of high-quality occultation profiles. These profiles, which include data from both GPS and GLONASS satellites, rising and setting occultations, have exceeded the mission's performance targets.

This study utilized a dataset from the last four months of 2021 to evaluate the ability of the Sentinel-6A RO processor version 4.0 to provide high quality bending angle profiles. This version is scheduled to be deployed in operation environment the second quarter of 2024.

The Sentinel-6A RO receiver tracked signals analysis reveals that GPS signals exhibit relatively stable SNR values across different satellites, indicating consistent tracking capabilities for both L1 and L2 GPS signals. In contrast, GLONASS signals show more variability in SNR, with certain satellites exhibiting lower SNR values, especially on the L1 frequency. Further examination of daily averaged SNR values highlighted the effects of satellite maneuvers, such as yaw flips, on tracking capabilities. The analysis also underscores the variability and sensitivity of GLONASS signal tracking to orbital geometries, contrasting with the more stable performance of GPS signals. Together with SNR, phase noise was also taken into account. Phase noise can distort the received signal, impacting the accuracy of atmospheric measurements. The analysis indicates that GLONASS occultations are tracked with lower phase noise compared to GPS, affecting the retrieval of bending angles in the upper troposphere.

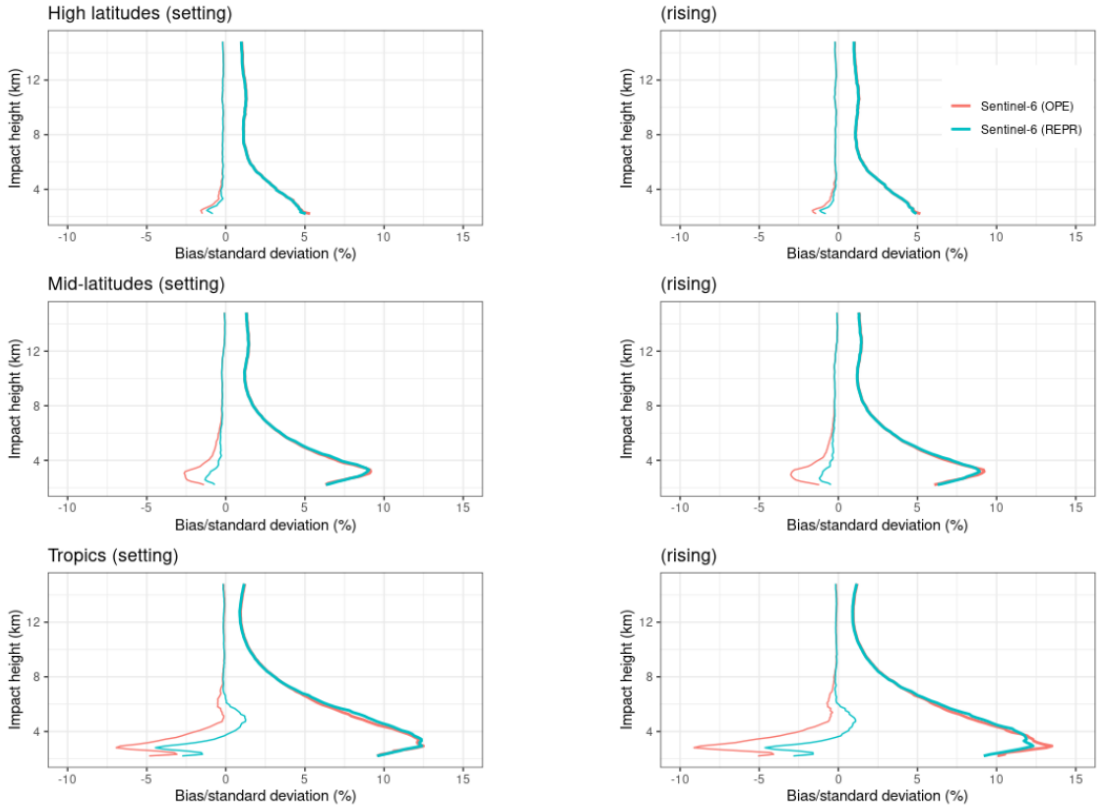

Figure 20. Global robust statistics of tropospheric operational and reprocessed Sentinel-6A bending angles compared against ECMWF short range forecasts during the analyzed period. The vertical profiles of biases (or systematic deviations) with think lines and respective standard deviations (or random deviations) are shown. Plots are stratified by latitudinal bands and split by rising and setting. High latitudes (60 deg, 90 deg N/S), Mid-latitudes (30 deg, 60 deg N/S), Tropics (-30 deg, 30 deg).

Investigations on RO data conducted post-launch, during the commissioning phase, addressed the issue of excessively noisy L2 frequency data in some tropospheric occultations. The procedure for extrapolating the L2 signal at lower altitudes using an ionospheric model based on a Chapman Layer to eliminate the ionospheric influence before merging the L1 and L2 bending angle profiles was improved. The determination of the L2 cutoff point was critical to enhance the accuracy and reliability of tropospheric data that accommodates varying solar activity conditions. An initial fixed threshold of 50μrad for the L2 signal cutoff, based on the L1-L2 bending angle difference, showed improvements in bending angle processing. An alternative approach of integrating the L2 cutoff into the bending angles ionospheric correction process was used. Actual data were robustly fitted into the ionospheric model in order to determine the reference for the L2 signal cutoff algorithm. This new approach was shown to bring substantial improvements into the random errors of the presented statistics.

The determination of the optimal cut-off points for L1 and L2 GNSS signals based on their SNR levels is a key point for processing data recorded by Open-Loop RO receivers. Different cutoff heights introduce variations in tropospheric bias

structure when RO profiles are compared against ECMWF data. The EUMETSAT RO NTC processor employs the SNR-based signal cutoff algorithm as detailed in Sokolovskiy et al. (2010), with minor modifications to address the zero amplitude/SNR occurrences regularly noted in L2 data from JPL receivers, leading to a tropospheric bias shift of about 1%.

The improvements made to the Sentinel-6A RO-NTC processor for effectively removing navigation bits from the received L1/L2 GNSS signals are discussed. The enhancements have resulted in better-quality bending angle profiles, as demonstrated by comparisons with ECMWF models, showing improved performance in the lower stratosphere and troposphere for GLONASS signals and across all altitudes for GPS signals. This has contributed to an overall improvement in the data quality produced by the Sentinel-6 RO NTC processor.

Interference signals on the I and Q components of the L2 frequency, not related to GNSS navigation bits, were discussed. Interference at 40/20 Hz was specifically noted in the SNR spectrum of the L2 signals. This phenomenon is more frequent when the satellite flies over the boundary between Russia and America, suggesting a possible geographic localization of the interference sources. Although such interference could potentially affect the data accuracy, the Sentinel-6 observations indicate that these signals did not significantly affect the receiver's performance.

Operational and reprocessed Sentinel-6A bending angles profiles were compared against ECMWF short-range forecasts. Operational and Reprocessed GRAS B/C and Spire RO profiles were also used for comparisons purposes. A general agreement between Sentinel-6A bending angle profiles and ECMWF profiles, similar to that between GRAS and ECMWF, is reported. This alignment underscores the ability of the EUMETSAT RO processors in maintaining consistent and high-quality data across different missions. The comparison also highlighted enhancements in the reprocessed data, which showed reduced random errors and improved adjustments in tropospheric biases. These improvements were primarily attributed to the refinements in the navigation bits removal algorithm and the implementation of an efficient signal cut-off strategy.

Competing interests. The contact author has declared that none of the authors has any competing interests

References

Anthes, R. A.: Exploring Earth's atmosphere with radio occultation: contributions to weather, climate and space weather, Atmospheric Measurement Techniques, 4, 1077–1103, https://doi.org/10.5194/amt-4-1077-2011, 2011.

Ao, C. O., Hajj, G. A., Meehan, T. K., Dong, D., Iijima, B. A., Mannucci, A. J., and Kursinski, E. R.: Rising and setting GPS occultations by use of open-loop tracking, Journal of Geophysical Research: Atmospheres, 114, https://doi.org/https://doi.org/10.1029/2008JD010483, 2009.

Cardinali, C. and Healy, S.: Impact of GPS radio occultation measurements in the ECMWF system using adjoint-based diagnostics, Quarterly Journal of the Royal Meteorological Society, 140, 2315–2320, https://doi.org/https://doi.org/10.1002/qj.2300, 2014.

Consortium, T. R. S.: The Radio Occultation Processing Package (ROPP) Forward Model Module User Guide, Radio Occultation Meteorology Satellite Application Facility (ROM-SAF), https://rom-saf.eumetsat.int/romsaf_ropp_ug_fm.pdf, 2021.

Culverwell, I. D. and Healy, S. B.: Simulation of L1 and L2 bending angles with a model ionosphere, Report 17, Radio Occultation Meteorology Satellite Application Facility (ROM-SAF), available online at https://rom-saf.eumetsat.int/general-documents/rsr/rsr_17.pdf, 2015.

Dach, R., Lutz, S., Walser, P., and Fridez, P.: Bernese GNSS Software Version 5.2, User manual, Astronomical Institute, University of Bern, Sidlerstrasse 5, CH–3012 Bern, Switzerland, https://doi.org/10.7892/boris.72297, 2015.

Danzer, J., Scherllin-Pirscher, B., and Foelsche, U.: Systematic residual ionospheric errors in radio occultation data and a potential way to minimize them, Atmospheric Measurement Techniques, 6, 2169–2179, https://doi.org/10.5194/amt-6-2169-2013, 2013.

Danzer, J., Healy, S. B., and Culverwell, I. D.: A simulation study with a new residual ionospheric error model for GPS radio occultation climatologies, Atmospheric Measurement Techniques, 8, 3395–3404, https://doi.org/10.5194/amt-8-3395-2015, 2015.

Donlon, C., Cullen, R., Giulicchi, L., Fornari, M., and Vuilleumier, P.: Copernicus Sentinel-6 Michael Freilich Satellite Mission: Overview and Preliminary in Orbit Results, in: 2021 IEEE International Geoscience and Remote Sensing Symposium IGARSS, pp. 7732–7735, https://doi.org/10.1109/IGARSS47720.2021.9553731, 2021a.

Donlon, C. J., Cullen, R., Giulicchi, L., Vuilleumier, P., Francis, C. R., Kuschnerus, M., Simpson, W., Bouridah, A., Caleno, M., Bertoni, R., Rancaño, J., Pourier, E., Hyslop, A., Mulcahy, J., Knockaert, R., Hunter, C., Webb, A., Fornari, M., Vaze, P., Brown, S., Willis, J., Desai, S., Desjonqueres, J.-D., Scharroo, R., Martin-Puig, C., Leuliette, E., Egido, A., Smith, W. H., Bonnefond, P., Le Gac, S., Picot, N., and Tavernier, G.: The Copernicus Sentinel-6 mission: Enhanced continuity of satellite sea level measurements from space, Remote Sensing of Environment, 258, 112 395, https://doi.org/https://doi.org/10.1016/j.rse.2021.112395, 2021b.

Esterhuizen, S., Franklin, G. W., Hurst, K. J., Mannucci, A. J., Meehan, T. K., Webb, F. H., and Young, L. E.: TriG - A GNSS Precise Orbit and Radio Occultation Space Receiver, https://api.semanticscholar.org/CorpusID:18240040, 2009.

Fjeldbo, G., Kliore, A. J., and Eshleman, V. R.: The neutral atmosphere of Venus as studied with the Mariner V radio occultation experiments, The Astronomical Journal, 76, 123, https://api.semanticscholar.org/CorpusID:120896341, 1971.

Fu, L.-L., Christensen, E. J., Yamarone Jr., C. A., Lefebvre, M., Ménard, Y., Dorrer, M., and Escudier, P.: TOPEX/POSEIDON mission overview, Journal of Geophysical Research: Oceans, 99, 24 369–24 381, https://doi.org/https://doi.org/10.1029/94JC01761, 1994.

Gill, E., Morton, J., Axelrad, P., Akos, D. M., Centrella, M., and Speretta, S.: Overview of Space-Capable Global Navigation Satellite Systems Receivers: Heritage, Status and the Trend towards Miniaturization, Sensors, 23, https://doi.org/10.3390/s23177648, 2023.

Gorbunov, M., Irisov, V., and Rocken, C.: The Influence of the Signal-to-Noise Ratio upon Radio Occultation Retrievals, Remote Sensing, 14, https://doi.org/10.3390/rs14122742, 2022a.

Gorbunov, M., Irisov, V., and Rocken, C.: Noise Floor and Signal-to-Noise Ratio of Radio Occultation Observations: A Cross-Mission Statistical Comparison, Remote Sensing, 14, https://doi.org/10.3390/rs14030691, 2022b.

Gorbunov, M. E.: Ionospheric correction and statistical optimization of radio occultation data, Radio Science, 37, 1–9, https://doi.org/10.1029/2000RS002370, 2002.

Gorbunov, M. E. and Lauritsen, K. B.: Analysis of wave fields by Fourier integral operators and their application for radio occultations, Radio Science, 39, https://doi.org/https://doi.org/10.1029/2003RS002971, 2004.

Hajj, G., Kursinski, E., Romans, L., Bertiger, W., and Leroy, S.: A technical description of atmospheric sounding by GPS occultation, Journal of Atmospheric and Solar-Terrestrial Physics, 64, 451–469, https://doi.org/https://doi.org/10.1016/S1364-6826(01)00114-6, 2002.

Harnisch, F., Healy, S. B., Bauer, P., and English, S. J.: Scaling of GNSS Radio Occultation Impact with Observation Number Using an Ensemble of Data Assimilations, Monthly Weather Review, 141, 4395 – 4413, https://doi.org/10.1175/MWR-D-13-00098.1, 2013.

Healy, S. B. and Culverwell, I. D.: A modification to the standard ionospheric correction method used in GPS radio occultation, Atmospheric Measurement Techniques, 8, 3385–3393, https://doi.org/10.5194/amt-8-3385-2015, 2015.

Ho, S.-P., Anthes, R. A., Ao, C. O., Healy, S., Horanyi, A., Hunt, D., Mannucci, A. J., Pedatella, N., Randel, W. J., Simmons, A., Steiner, A., Xie, F., Yue, X., and Zeng, Z.: The COSMIC/FORMOSAT-3 Radio Occultation Mission after 12 Years: Accomplishments, Remaining Challenges, and Potential Impacts of COSMIC-2, Bulletin of the American Meteorological Society, 101, E1107 – E1136, https://doi.org/10.1175/BAMS-D-18-0290.1, 2020.

Ho, S.-P., Zhou, X., Shao, X., Chen, Y., Jing, X., and Miller, W.: Using the Commercial GNSS RO Spire Data in the Neutral Atmosphere for Climate and Weather Prediction Studies, Remote Sensing, 15, https://doi.org/10.3390/rs15194836, 2023.

Hoaglin, D. C., Mosteller, F., and Tukey, J. W.: Understanding robust and exploratory data analysis, Wiley & Sons Ltd, New York, 2000.

Isoz, O., Buehler, S. A., Kinch, K., Bonnedal, M., and Akos, D. M.: Interference from terrestrial sources and its impact on the GRAS GPS radio occultation receiver, Radio Science, 49, 1–6, https://doi.org/10.1002/2013RS005243, 2014.

Jakowski, N., Angling, M., and Leitinger, R.: Radio Occultation Techniques for Probing the Ionosphere, Annals of Geophysics, 47, 1049–1066, https://doi.org/10.4401/ag-3285, 2009.

Jiang, M., Xu, K., and Wang, J.: Evaluation of Sentinel-6 Altimetry Data over Ocean, Remote Sensing, 15, https://doi.org/10.3390/rs15010012, 2023.

Kursinski, E. R., Hajj, G. A., Schofield, J. T., Linfield, R. P., and Hardy, K. R.: Observing Earth's atmosphere with radio occultation measurements using the Global Positioning System, Journal of Geophysical Research: Atmospheres, 102, 23 429–23 465, https://doi.org/https://doi.org/10.1029/97JD01569, 1997.

Kursinski, R., Hajj, G., Leroy, S., and Herman, B.: The GPS Radio Occultation Technique, Terrestrial, Atmospheric and Oceanic Sciences, 11, 53–, https://doi.org/10.3319/TAO.2000.11.1.53(COSMIC), 2001.

Melbourne, W., Davis, E., Duncan, C., Hajj, G., Hardy, K., Kursinski, E., Meehan, T., Young, L., and Yunck, T.: The application of spaceborne GPS to atmospheric limb sounding and global change monitoring, Tech. rep., 1994.

Mohamady, L. and Amiri, S. a.: Performance Analysis of Different Frequency Estimation Methods in GNSS-RO Receivers with Open Loop Tracking, The Modares Journal of Electrical Engineering, 13, http://mjee.modares.ac.ir/article-17-12288-en.html, 2013.

Padovan, S., Andres, Y., Paolella, S., Engeln, A. V., Notarpietro, R., Butenko, L., Alemany, F. M., Sancho, F., and Marquardt, C.: Impact of the GNSS clock rate on Radio Occultation bending angles, Atmospheric Measurement Techniques, 2024.

Smith, E. K. and Weintraub, S.: The Constants in the Equation for Atmospheric Refractive Index at Radio Frequencies, Proceedings of the IRE, 41, 1035–1037, https://api.semanticscholar.org/CorpusID:51668997, 1953.

Sokolovskiy, S., Rocken, C., Schreiner, W., Hunt, D., and Johnson, J.: Postprocessing of L1 GPS radio occultation signals recorded in open-loop mode, Radio Science, 44, https://doi.org/https://doi.org/10.1029/2008RS003907, 2009.

Sokolovskiy, S., Rocken, C., Schreiner, W., and Hunt, D.: On the uncertainty of radio occultation inversions in the lower troposphere, Journal of Geophysical Research: Atmospheres, 115, https://doi.org/https://doi.org/10.1029/2010JD014058, 2010.

Steiner, A., Kirchengast, G., Foelsche, U., Kornblueh, L., Manzini, E., and Bengtsson, L.: GNSS occultation sounding for climate monitoring, Physics and Chemistry of the Earth, Part A: Solid Earth and Geodesy, 26, 113–124, https://doi.org/https://doi.org/10.1016/S1464-1895(01)00034-5, 2001.

Tien, J., Young, L., Meehan, T., Franklin, G., Hurst, K., and Esterhuizen, S.: Next Generation of Spaceborne GNSS Receiver for Radio Occultation Science and Precision Orbit Determination, 2010.

von Engeln, A.: Jason-CS/Sentinel-6 RO Level 1B Auxiliary Data Specification, Auxiliary Data Specification document v3G, EUMETSAT, Darmstadt, 2022a.

von Engeln, A.: Jason-CS/Sentinel-6 RO Level 1B Product Format Specification, Product Format Specification document v3F, EUMETSAT, Darmstadt, 2022b.

von Engeln, A.: Jason-CS/Sentinel-6 RO Level 1B NTC Product Generation Specification, Product Generation Specification document v3F, EUMETSAT, Darmstadt, 2022c.

von Engeln, A.: Sentinel-6 A GNSS-RO NTC Cal/Val Report, Calibration and Validation Report v1E, EUMETSAT, Darmstadt, 2024.

Withers, P.: Prediction of uncertainties in atmospheric properties measured by radio occultation experiments, Advances in Space Research, 46, 58–73, https://doi.org/https://doi.org/10.1016/j.asr.2010.03.004, 2010.

Yen, N. L., Fong, C.-J., Chu, C.-H., Miau, J.-J., Liou, Y.-A., , and Kuo, Y.-H.: Global GNSS Radio Occultation Mission for Meteorology, Ionosphere & Climate, in: Aerospace Technologies Advancements, edited by Arif, T. T., chap. 13, IntechOpen, Rijeka, https://doi.org/10.5772/6928, 2010.